Inorg. Chem. **2005**, *44*, 133–146

Framework Control by a Metalloligand Having Multicoordination Ability: New Synthetic Approach for Crystal Structures and Magnetic Properties

Shin-ichiro Noro,[†,‡] Hitoshi Miyasaka,[§] Susumu Kitagawa,*[,∥] Tatsuo Wada,[†] Takashi Okubo,[⊥] Masahiro Yamashita,[§] and Tadaoki Mitani[⊥]

Supramolecular Science Laboratory, RIKEN (The Institute of Physical and Chemical Research), Hirosawa 2-1, Wako, Saitama 351-0198, Japan, Department of Synthetic Chemistry and Biological Chemistry, Graduate School of Engineering, Kyoto University, Katsura, Nishikyo-ku, Kyoto 615-8510, Japan, Department of Chemistry, Graduate School of Science, Tokyo Metropolitan University, Minami-Ohsawa 1-1, Hachioji, Tokyo 192-0397, Japan, and Department of Physical Materials Science, School of Materials Science, Japan Advanced Institute of Science & Technology, Tatsunokuchi, Ishikawa 923-1292, Japan

Received April 5, 2004

By utilizing the novel metalloligand L^{Cu}, $[Cu(2,4\text{-pydca})_2]^{2-}$ (2,4-pydca^{2-} = pyridine-2,4-dicarboxylate), which possesses two kinds of coordination groups, selective bond formation with the series of the first-period transition metal ions (Mn^{II}, Fe^{II}, Co^{II}, Cu^{II}, and Zn^{II}) has been accomplished. Depending on the coordination mode of 4-carboxylate with Co^{II}, Cu^{II}, and Zn^{II} ions, L^{Cu} forms a one-dimensional (1-D) assembly with a repeating motif of [–M–O_2C–(py)N–Cu–N(py)–CO_2–]: $\{[ZnL^{Cu}(H_2O)_3(DMF)]\cdot DMF\}_n$ (**2**), $[ZnL^{Cu}(H_2O)_2(MeOH)_2]_n$ (**3**), and $\{[ML^{Cu}(H_2O)_4]\cdot 2H_2O\}_n$ (M = Co (**4**), Cu (**5**), Zn (**6**)). The use of a terminal ligand of 2,2′-bipyridine (2,2′-bpy), in addition to the Cu^{II} ion, gives a zigzag 1-D assembly with the similar repeating unit as **4**–**6**: $\{[Cu(2,2'\text{-bpy})L^{Cu}]\cdot 3H_2O\}_n$ (**9**). On the other hand, for Mn^{II} and Fe^{II} ions, L^{Cu} shows a 2-carboxylate bridging mode to form an another 1-D assembly with a repeating motif of [–M–O–C–O–Cu–O–C–O–]: $[ML^{Cu}(H_2O)_4]_n$ (M = Mn (**7**), Fe (**8**)). This selectivity is related to the strength of Lewis basicity and the electrostatic effect of L^{Cu} and the Irving–Williams order on the present metal ions. According to their bridging modes, a variety of magnetic properties are obtained: **4**, **5**, and **9**, which have the 4-carboxypyridinate bridge between magnetic centers, have weak antiferromagnetic interaction, whereas **7** and **8** with the carboxylate bridge between magnetic centers reveal 1-D ferromagnetic behavior (Cu^{II}–M^{II}; M^{II} = Mn^{II}, J/k_B = 0.69 K for **7**; M^{II} = Fe^{II}, J/k_B = 0.71 K for **8**).

Introduction

The chemistry of coordination polymers is of great interest because of their structural diversities[1] and unique functionalities such as host−guest chemistry,[2] magnetism,[3] electronic conductivity,[4] and optical property.[5] On current synthetic methodologies of such coordination polymers, the choice of building blocks is of significant at initial stage of preparations. The transition metal ions themselves could be the simplest building blocks, which provide various spatial and electronic structures in accord with their coordination numbers, geometries, and oxidation and spin states; the metal ions participate in nodes of dimensional grids. On the

* To whom correspondence should be addressed. E-mail: kitagawa@sbchem.kyoto-u.ac.jp.
[†] RIKEN.
[‡] Present address: Research Institute for Electronic Science, Hokkaido University, Sapporo 060-0812, Japan.
[§] Tokyo Metropolitan University.
[∥] Kyoto University.
[⊥] Japan Advanced Institute of Science & Technology.

(1) (a) Zaworotko, M. J. *Chem. Soc. Rev.* **1994**, 283−288. (b) Batten, S. R.; Robson, R. *Angew. Chem., Int. Ed.* **1998**, *37*, 1460−1494. (c) Hagrman, P. J.; Hagrman, D.; Zubieta, J. *Angew. Chem., Int. Ed.*. **1999**, *38*, 2638−2684. (d) Blake, A. J.; Champness, N. R.; Hubberstey, P.; Li, W.-S.; Withersby, M. A.; Schröder, M. *Coord. Chem. Rev.* **1999**, *183*, 117−138. (e) Robson, R. *J. Chem. Soc., Dalton Trans.* **2000**, 3735−3744. (f) Moulton, B.; Zaworotko, M. J. *Chem. Rev.* **2001**, *101*, 1629−1658. (g) Zaworotko, M. J. *Chem. Commun.* **2001**, 1−9. (h) Kim, K. *Chem. Soc. Rev.* **2002**, *31*, 96−107. (i) Khlobystov, A. N.; Blake, A. J.; Champness, N. R.; Lemenovskii, D. A.; Majouga, A. G.; Zyk, N. V.; Schröder, M. *Coord. Chem. Rev.* **2001**, *222*, 155−192.

(2) (a) Kitagawa, S.; Kondo, M. *Bull. Chem. Soc. Jpn.* **1998**, *71*, 1739−1753. (b) Yaghi, O. M.; O'Keeffe, M.; Ockwig, N. W.; Chae, H. K.; Eddaoudi, M.; Kim, J. *Nature* **2003**, *423*, 705−714. (c) James, S. L. *Chem. Soc. Rev.* **2003**, *32*, 276−288. (d) Janiak, C. *Dalton Trans.* **2003**, 2781−2804.

10.1021/ic049550e CCC: $30.25
Published on Web 12/03/2004

contrary, organic bridging ligands generally construct backbones for the fabrication of a coordination network. Combinations of these building blocks have succeeded to form a wide variety of molecular architectures. More controlled fabrication to desire fruitful structures and novel physical properties would be achieved by using metal complexes as building blocks, sometimes called "metalloligands". A metalloligand has several advantages to design infinite frameworks: (i) multicoordination sites (functional groups), (ii) polyhedral coordination-donor building block controlled in coordination-direction, and (iii) easy to construct heterometallic assembly systems. The representative metalloligands refer to $[M^{III}(CN)_x]^{3-x}$ and $[M^{III}(ox)_3]^{3-}$ (ox^{2-} = oxalate). Their assemblies have been in the spotlight to date;[3e,6] however, reports on coordination polymers with metalloligands are still sparse in comparison with pure organic ligands.[3b,e,7] Another famous example of a metalloligand may be Cu^{II} complexes reported by Kahn's group,[7g−k,8] where the metalloligands containing oxamate, oxamide, benzoate, or propionate groups bridge second transition metal ions of Mn^{II}, Co^{II}, Ni^{II}, and Cu^{II} to form heterometallic coordination polymers indicating interesting magnetic behavior with a long-range order.

Our desirable metalloligand is one that possesses multicoordination ability in addition to the above-mentioned peculiarities i−iii. We have recently developed a new metalloligand, $(Et_3NH)_2[Cu(2,4\text{-pydca})_2(H_2O)]$ (**1**·2Et_3NH) (2,4-pydca^{2-} = pyridine-2,4-dicarboxylate), prepared by the reaction of $[Cu(2,4\text{-pydcaH})_2(H_2O)_2]$ (**1**·2H) with Et_3N.[9] The metalloligand $[Cu(2,4\text{-pydca})_2]^{2-}$ (hereafter, $[Cu(2,4\text{-pydca})_2]^{2-}$ is abbreviated as L^{Cu}) has two kinds of Lewis-base coordination groups, 4-carboxylate (group A) and 2-carboxylate (group B) moieties, as shown in Chart 1. Group A is a regular carboxylate linker, whereas group B contributes to both chelating of the central Cu^{II} ion (formation of the metalloligand) and bridging with other metal ions presented. The bridging capability of group B is thus weaker than that of group A because of its weak electron-donating and electrostatic power. Indeed, $\{[ZnL^{Cu}(H_2O)_3(DMF)]\cdot DMF\}_n$ (**2**) and $[ZnL^{Cu}(H_2O)_2(MeOH)_2]_n$ (**3**) synthesized previously revealed the 4-carboxylate bridging mode (the 4-carboxylate group of L^{Cu} linked Zn^{II} ions but the 2-carboxylate group was coordination-free for Zn^{II} ions).[9] From this aspect, our interest was directed to the selectivity of coordination groups in a metalloligand for a certain metal ion. If the control of the choice of metal ions for coordination groups, namely what we call "bond engineering in metalloligand", is possible, we could obtain not only important information toward a rational synthetic strategy for coordination polymers, but also desired

Chart 1

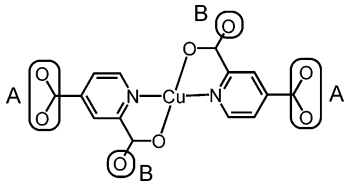

(3) (a) Kahn, O. *Molecular Magnetism*; VCH: New York, 1993. (b) Clérac, R.; Miyasaka, H.; Yamashita, M.; Coulon, C. *J. Am. Chem. Soc.* **2002**, *124*, 12837−12844. (c) Caneschi, A.; Gatteschi, D.; Lalioti, N.; Sangregorio, C.; Sessoli, R.; Venturi, G.; Vindigni, A.; Rettori, A.; Pini, M. G.; Novak, M. A. *Angew. Chem., Int. Ed.* **2001**, *40*, 1760−1763. (d) Miyasaka, H.; Matsumoto, N.; Okawa, H.; Re, N.; Gallo, E.; Floriani, C. *J. Am. Chem. Soc.* **1996**, *118*, 981−994. (e) Tamaki, J.; Zhong, Z. J.; Matsumoto, N.; Kida, S.; Koikawa, M.; Achiwa, N.; Hashimoto, Y.; Okawa, H. *J. Am. Chem. Soc.* **1992**, *114*, 6974−6979. (f) Coronado, E.; Galan-Mascaros, J. R.; Gomez-Garcia, C. J.; Laukhin, V. *Nature* **2000**, *408*, 447−449. (g) Miller, J. S.; Calabrese, J. C.; McLean, R. S.; Epstein, A. J. *Adv. Mater.* **1992**, *4*, 498−501.

(4) (a) Sinzger, K.; Hünig, S.; Jopp, M.; Bauer, D.; Beitsch, W.; von Schütz, J. U.; Wolf, H. C.; Kremer, R. K.; Metzenthin, T.; Bau, R.; Khan, S. I.; Lindbaum, A.; Lengauer, C. L.; Tillmanns, E. *J. Am. Chem. Soc.* **1993**, *115*, 7696−7705. (b) Aumüller, A.; Erk, P.; Klebe, G.; Hünig, S.; von Schütz, J. U.; Werner, H.-P. *Angew. Chem., Int. Ed. Engl.* **1986**, *25*, 740−741. (c) Hünig, S.; Kemmer, M.; Meixner, H.; Sinzger, K.; Wenner, H.; Bauer, T.; Tillmanns, E.; Lux, F. R.; Hollstein, M.; Gross, H.-G.; Langohr, U.; Werner, H.-P.; von Schütz, J. U.; Wolf, H.-C. *Eur. J. Inorg. Chem.* **1999**, 899−916. (d) Kato, R.; Kobayashi, H.; Kobayashi, A. *J. Am. Chem. Soc.* **1989**, *111*, 5224−5232. (e) Kitagawa, H.; Onodera, N.; Sonoyama, T.; Yamamoto, M.; Fukawa, T.; Mitani, T.; Seto, M.; Maeda, Y. *J. Am. Chem. Soc.* **1999**, *121*, 10068−10080.

(5) (a) Evans, O. R.; Lin, W. *Acc. Chem. Res.* **2002**, *35*, 511−522. (b) Janiak, C.; Scharmann, T. G.; Albrecht, P.; Marlow, F.; Macdonald, R. *J. Am. Chem. Soc.* **1996**, *118*, 6307−6308. (c) Shi, J.-M.; Xu, W.; Liu, Q.-Y.; Liu, F.-L.; Huang, Z.-L.; Lei, H.; Yu, W.-T.; Fang, Q. *Chem. Commun.* **2002**, 756−757. (d) Kisida, H.; Matsuzaki, H.; Okamoto, H.; Manabe, T.; Yamashita, M.; Taguchi, Y.; Tokura, Y. *Nature* **2000**, *405*, 929−932. (e) Hou, H.; Meng, X.; Song, Y.; Fan, Y.; Zhu, Y.; Lu, H.; Du, C.; Shao, W. *Inorg. Chem.* **2002**, *41*, 4068−4075.

(6) (a) Okawa, H.; Ohba, M. *Bull. Chem. Soc. Jpn.* **2002**, *75*, 1191−1203. (b) Dunbar, K. R.; Heintz, R. A. *Prog. Inorg. Chem.* **1997**, *45*, 283−391. (c) Tamaki, H.; Mitsumi, M.; Nakamura, K.; Matsumoto, N.; Kida, S.; Okawa, H.; Iijima, S. *Chem. Lett.* **1992**, 1975−1978. (d) Mathonière, C.; Nuttall, C. J.; Carling, S. G.; Day, P. *Inorg. Chem.* **1996**, *35*, 1201−1206.

(7) (a) Sugimoto, K.; Kuroda-Sowa, T.; Maekawa, M.; Munakata, M. *J. Chem. Soc., Chem. Commun.* **1999**, 455−456. (b) Chang, W.-K.; Sheu, S.-C.; Lee, G.-H.; Wang, Y.; Ho, T.-I.; Lin, Y.-C. *J. Chem. Soc., Dalton Trans.* **1993**, 687−694. (c) Miah, M. A. A.; Phillips, D. J.; Rae, A. D. *Inorg. Chim. Acta* **1996**, *245*, 231−235. (d) Gleizes, A.; Verdaguer, M. *J. Am. Chem. Soc.* **1984**, *106*, 3727−3737. (e) Ruiz, R.; Julve, M.; Faus, J.; Lloret, F.; Muñoz, M. C.; Journaux, Y.; Bois, C. *Inorg. Chem.* **1997**, *36*, 3434−3439. (f) Xu, D.; Gu, J.; Xu, L.; Liang, K.; Xu, Y. *Polyhedron* **1998**, *17*, 231−233. (g) Pei, Y.; Kahn, O.; Sletten, J. *J. Am. Chem. Soc.* **1986**, *108*, 3143−3145. (h) Pei, Y.; Kahn, O.; Sletten, J.; Renard, J.-P.; Georges, R.; Gianduzzo, J.-C.; Curely, J.; Xu, Q. *Inorg. Chem.* **1988**, *27*, 47−53. (i) Kahn, O.; Pei, Y.; Verdaguer, M.; Renard, J. P.; Sletten, J. *J. Am. Chem. Soc.* **1988**, *110*, 782−789. (j) Stumpf, H. O.; Ouahab, L.; Pei, Y.; Grandjean, D.; Kahn, O. *Science* **1993**, *261*, 447−449. (k) Lloret, F.; Julve, M.; Ruiz, R.; Journaux, Y.; Nakatani, K.; Kahn, O.; Sletten, J. *Inorg. Chem.* **1993**, *32*, 27−31. (l) Nakatani, K.; Sletten, J.; Halut-Desporte, S.; Jeannin, S.; Jeannin, Y.; Kahn, O. *Inorg. Chem.* **1991**, *30*, 164−171. (m) Pei, Y.; Nakatani, K.; Kahn, O.; Sletten, J.; Renard, J. P. *Inorg. Chem.* **1989**, *28*, 3170−3175. (n) Ciurtin, D. M.; Smith, M. D.; zur Loye, H.-C. *Chem. Commun.* **2002**, 74−75. (o) Dong, Y.-B.; Smith, M. D.; zur Loye, H.-C. *Inorg. Chem.* **2000**, *39*, 1943−1949. (p) Dong, Y.-B.; Smith, M. D.; zur Loye, H.-C. *Angew. Chem., Int. Ed.* **2000**, *39*, 4271−4273. (q) Carlucci, L.; Ciani, G.; Porta, F.; Proserpio, D. M.; Santagostini, L. *Angew. Chem., Int. Ed.* **2002**, *41*, 1907−1911.

(8) (a) Pei, Y.; Verdaguer, M.; Kahn, O. *J. Am. Chem. Soc.* **1986**, *108*, 7428−7430. (b) Pei, Y.; Verdaguer, M.; Kahn, O.; Sletten, J.; Renard, J.-P. *Inorg. Chem.* **1987**, *26*, 138−143. (c) Stumpf, H. O.; Pei, Y.; Kahn, O.; Sletten, J.; Renard, J. P. *J. Am. Chem. Soc.* **1993**, *115*, 6738−6745. (d) Stumpf, H. O.; Pei, Y.; Ouahab, L.; Le Berre, F.; Codjovi, E.; Kahn, O. *Inorg. Chem.* **1993**, *32*, 5687−5691. (e) Gulbrandsen, A.; Sletten, J.; Nakatani, K.; Pei, Y.; Kahn, O. *Inorg. Chim. Acta* **1993**, *212*, 271−279. (f) Stumpf, H. O.; Ouahab, L.; Pei, Y.; Bergerat, P.; Kahn, O. *J. Am. Chem. Soc.* **1994**, *116*, 3866−3874. (g) Baron, V.; Gillon, B.; Sletten, J.; Mathoniere, C.; Codjovi, E.; Kahn, O. *Inorg. Chim. Acta* **1995**, *235*, 69−76. (h) Baron, V.; Gillon, B.; Cousson, A.; Mathonière, C.; Kahn, O.; Grand, A.; Öhrström, L.; Delley, B.; Bonnet, M.; Boucherle, J.-X. *J. Am. Chem. Soc.* **1997**, *119*, 3500−3506.

(9) (a) Noro, S.; Kitagawa, S.; Yamashita, M.; Wada, T. *Chem. Commun.* **2002**, 222−223. (b) Noro, S.; Kitagawa, S.; Yamashita, M.; Wada, T. *CrystEngComm* **2002**, *4*, 162−164.

Scheme 1

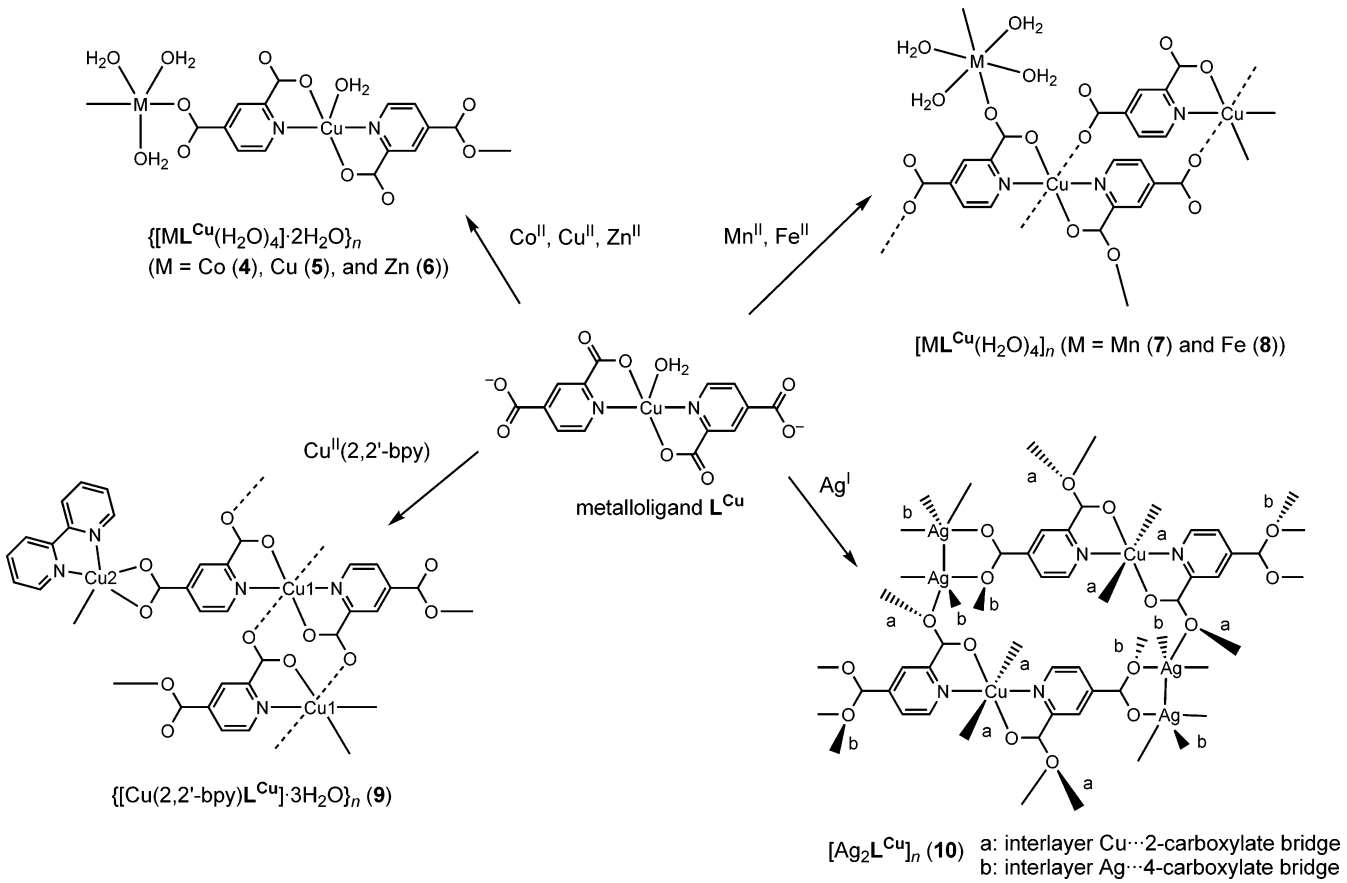

magnetic materials, properties of which are strongly dependent on bridging features between the Cu^{II} centers of L^{Cu} and second transition metal ions.

In this paper, we report a successful selective bond formation of coordination polymers, $\{[ML^{Cu}(H_2O)_4]\cdot 2H_2O\}_n$ (M = Co (**4**), Cu (**5**), Zn (**6**)), $[ML^{Cu}(H_2O)_4]_n$ (M = Mn (**7**), Fe (**8**)), and $\{[Cu(2,2'\text{-bpy})L^{Cu}]\cdot 3H_2O\}_n$ (**9**) (2,2′-bpy = 2,2′-bipyridine). These compounds are constructed from the combination of the metalloligand **1**·2Et_3NH and corresponding metals (**4**−**8**) or a metal complex $[Cu(2,2'\text{-bpy})]^{2+}$ (**9**) as the second building unit (Scheme 1). L^{Cu} indicates the bonding selectivity for the first-period transition metal ions used and thereby controls the magnetic properties of obtained coordination polymers as well. With another coordination polymer of $[Ag_2L^{Cu}]_n$ (**10**), their detailed structures and magnetic properties are discussed.

Results and Discussion

Preparation of the Metalloligands. Assembly of Cu^{II} ion with 2,4-pydcaH_2 (1:2 ratio) in a water/methanol solution afforded novel metalloligand **1**·2H with the monoanionic form, 2,4-pydcaH^-, without the presence of any deprotonation reagents. The IR spectrum of **1**·2H shows a ν(C═O) stretching band for the 4-CO_2H groups at 1728 cm^{-1} and ν_{as}(COO)/ν_s(COO) ones for the 2-CO_2^- groups at 1653/1367 cm^{-1}. Note that no polymeric compounds were obtained in this reaction condition. Nevertheless, this compound is scarcely soluble in common solvents such as water, alcohol, acetonitrile, DMF, $CHCl_3$, CH_2Cl_2, and diethyl ether, and this fact limits the utility of **1**·2H as a metalloligand. Therefore, an anionic metalloligand, **1**·2Et_3NH, was prepared by further deprotonation of the remaining 4-carboxylic acid parts of **1**·2H in the presence of Et_3N; **1**·2Et_3NH has only ν_{as}(COO)/ν_s(COO) stretching bands at 1658,1628/1369,1342 cm^{-1}. As expected, **1**·2Et_3NH is easily soluble in polar solvents such as water, MeOH, and DMF, being useful as a metalloligand. The difference of the solubility between the two types of the metalloligands could be ascribed to their hydrogen-bonding networks in the solid state (vide infra).

Crystal Structures of Metalloligands, $[Cu(2,4\text{-pydcaH})_2(H_2O)_2]$ (1·2H) and $(Et_3NH)_2[Cu(2,4\text{-pydca})_2(H_2O)]$ (1·2Et_3NH). ORTEP views around the Cu^{II} center of **1**·2H and **1**·2Et_3NH are shown in Figure 1a,b, respectively. Selected bond distances and angles are listed in Table 1. It should be noted that the structures of **1**·2H and **1**·2Et_3NH are characteristically different from each other in two aspects of the number of coordinated H_2O molecules and the protonation of 4-carboxylate groups. The Cu^{II} center of **1**·2H can be described as an axially elongated octahedron with two axial H_2O molecules and two nitrogen and two oxygen donors of the chelating 2,4-pydcaH^- ligands occupying the basal sites. Since there is an apparent difference between the two C−O bond distances of the 4-CO_2 groups (Table 2), they should be considered as an acidic type of −CO_2H. This fact is in good agreement with the IR data. Consequently, **1**·2H forms a neutral building block. The Cu^{II}

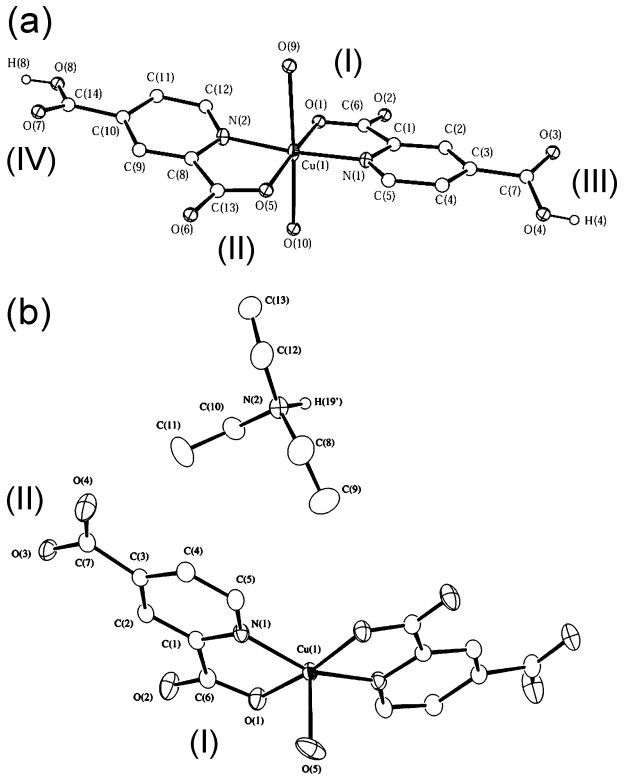

Figure 1. ORTEP drawing around a Cu^{II} center of (a) **1**·2H and (b) **1**·2Et_3NH at the 30% probability level. All hydrogen atoms except for COOH parts of **1**·2H and triethylammonium proton of **1**·2Et_3NH are omitted for clarity. Roman numerals I−IV are used to briefly describe each carboxylate part.

ion of **1**·2Et_3NH is a distorted square-pyramid with an apical H_2O molecule and two nitrogen and two oxygen atoms of 2,4-pydca^{2-} in the basal plane. In contrast to **1**·2H, the two C−O bond distances of the 4-CO_2 groups of **1**·2Et_3NH are similar to each other (Table 2), indicative of their anionic form, $-CO_2^-$, which is consistent with the IR data. The countercation for the anionic metalloligand, $[Cu(2,4\text{-pydca})_2(H_2O)]^{2-}$, is protonated Et_3N molecules, $(Et_3NH)^+$, as shown in the X-ray crystallographic data (N−H = 0.98 Å and O_{-COO}−H = 1.71 Å). These compounds form hydrogen-bonding networks, the dimension of which is varied in accord with the aforementioned structural characters. In the case of **1**·2H, the 4-carboxylic acid groups form intermolecular hydrogen bonds with the coordinated H_2O molecules with an average bond distance of 2.590 Å, and the coordination-free oxygen atoms of the 2-carboxylate groups also link to the coordinated H_2O molecules in another hydrogen-bonding mode (av 2.730 Å) as shown in Figure 2a, forming a three-dimensional (3-D) hydrogen-bonding network. In **1**·2Et_3NH, the 4-carboxylate groups make intermolecular hydrogen bonds with the coordinated H_2O molecules (2.679(2) Å) and free $(Et_3NH)^+$ molecules (2.683(2) Å). However, there is no hydrogen-bonding interaction with the coordination-free oxygen atoms of the 2-carboxylate groups, being in sharp contrast to that of **1**·2H. The **1**·2Et_3NH unit forms a one-dimensional (1-D) hydrogen-bonding network (Figure 2b). Both compounds also form the $\pi-\pi$ interactions between pyridinedicarboxylate parts (C···C = 3.6 Å and C···O = 3.1−3.5 Å for **1**·2H, and C···C = 3.6 Å and C···O = 3.6 Å for **1**·2Et_3NH). These $\pi-\pi$ interactions spread in the direction of one dimension. Considering that a $\pi-\pi$ interaction is generally weaker that a hydrogen-bonding one, the dimensionality of hydrogen-bonding network could be closely related to the solubility of **1**·2H and **1**·2Et_3NH as mentioned in the previous section. Note that the coordination geometry of a basic unit $[Cu(2,4\text{-pydca})_2]^{2-}$ (L^{Cu}), taking a Jahn−Teller geometry with the equatorial 2,4-pydca^{2-} ligands, is preserved even in extended polymer structures of **2**−**10** (vide infra).

Crystal Structures of 1-D Chain Polymers, $\{[ML^{Cu}(H_2O)_4]\cdot 2H_2O\}_n$ (M = Co (4), Cu (5), Zn (6)). Compounds **4**−**6** are isomorphous as a coordination 1-D polymer, in which the metalloligand L^{Cu} acts as a linear-type bridge. An ORTEP view around the metal centers of **4** is representatively shown in Figure 3a. Selected bond distances and angles of **4**−**6** are summarized in Table 3. The coordination environment of each Cu^{II} center of the metalloligand L^{Cu} consists of an apical H_2O molecule and two sets of N_2O_2 donor atoms of 2,4-pydca^{2-} chelating ligands in the basal plane, forming a distorted square pyramid as observed in the precursor **1**·2Et_3NH. The Co^{II} center also has a distorted square

Table 1. Selected Bond Distances (Å) and Angles (deg) of **1**·2H and **1**·2Et_3NH[a]

(a) $[Cu(2,4\text{-pydcaH})_2(H_2O)_2]$ (**1**·2H) Distances

Cu(1)−O(1)	1.946(2)	Cu(1)−O(5)	1.943(2)	Cu(1)−O(9)	2.684(2)
Cu(1)−O(10)	2.524(2)	Cu(1)−N(1)	1.979(2)	Cu(1)−N(2)	1.979(2)

Angles

O(1)−Cu(1)−O(5)	174.83(8)	O(1)−Cu(1)−O(9)	96.30(7)
O(1)−Cu(1)−O(10)	85.10(7)	O(1)−Cu(1)−N(1)	83.25(8)
O(1)−Cu(1)−N(2)	96.49(8)	O(5)−Cu(1)−O(9)	88.84(7)
O(5)−Cu(1)−O(10)	89.74(7)	O(5)−Cu(1)−N(1)	97.30(8)
O(5)−Cu(1)−N(2)	83.54(8)	O(9)−Cu(1)−O(10)	177.50(5)
O(9)−Cu(1)−N(1)	90.31(8)	O(9)−Cu(1)−N(2)	83.22(8)
O(10)−Cu(1)−N(1)	91.91(7)	O(10)−Cu(1)−N(2)	94.57(8)
N(1)−Cu(1)−N(2)	173.46(8)		

(b) $\{[Cu(2,4\text{-pydca})_2(H_2O)]\cdot 2Et_3NH\}$ (**1**·2Et_3NH) Distances

Cu(1)−O(1)	1.938(1)	Cu(1)−O(5)	2.141(2)	Cu(1)−N(1)	2.001(1)

Angles

O(1)−Cu(1)−O(1*)	168.57(8)	O(1)−Cu(1)−O(5)	95.71(4)
O(1)−Cu(1)−N(1)	82.85(5)	O(1)−Cu(1)−N(1*)	94.77(5)
O(5)−Cu(1)−N(1)	101.95(4)	N(1)−Cu(1)−N(1*)	156.09(9)

[a] Symmetry code: (*) $2-x, y, {}^2/_3-z$.

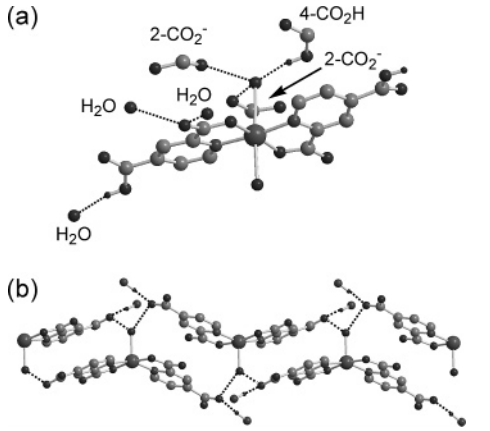

Figure 2. (a) View of the hydrogen-bonding mode of **1**·2H. All hydrogen atoms except for the COOH parts are omitted for clarity. Only a half part of the hydrogen-bonding mode is shown for simplicity. The dotted lines indicate hydrogen bonds. (b) View of the 1-D hydrogen-bonding network of **1**·2Et_3NH. The ethyl substituents of $(Et_3NH)^+$ and all hydrogen atoms except for triethylammonium protons are omitted for clarity. The dotted lines indicate hydrogen bonds.

Table 2. C−O Bond Distances, Difference, and Charge Type for **1**·2H and **1**·2Et_3NH

compd		bond length (Å)	difference (Å)	type
1·2H	I	1.265(3), 1.240(3)	0.025	carboxylate
	II	1.261(3), 1.240(3)	0.021	carboxylate
	III	1.317(3), 1.207(3)	0.110	carboxylic acid
	IV	1.311(3), 1.202(4)	0.109	carboxylic acid
1·2Et_3NH	I	1.285(2), 1.210(2)	0.075	carboxylate
	II	1.256(2), 1.215(2)	0.041	carboxylate

pyramidal geometry surrounded by one apical oxygen donor of H_2O molecule and four equatorial oxygen donors given from two other H_2O molecules and two 4-carboxylate groups of L^{Cu}, forming an alternating linear 1-D chain (Figure 3b). The average distance between the Co^{II} centers and the coordination oxygen of 4-carboxylate bridges is 1.975 Å, which is regularly observed in the metal−carboxylate bonding mode. Each chain connects itself with neighboring chains by interchain hydrogen bonds between M-coordinated H_2O molecules and oxygen atoms of 2-carboxylate groups, and between Co-coordinated H_2O molecules and oxygen atoms of 4-carboxylate groups with the bond distances of 2.68−2.88 Å as shown in Figure 3c. The intrachain Cu···Co distance is ca. 8.80 Å, while the shortest interchain Cu···Cu and Co···Co distances are ca. 5.34 and 4.43 Å, respectively. The $\pi-\pi$ interactions between the pyridinedicarboxylate parts also support an interchain assembly (C···C = 3.4−3.6 Å and C···O = 3.2 Å).

Crystal Structures of 2-D Polymers, $\{[ZnL^{Cu}(H_2O)_3(DMF)]\cdot DMF\}_n$ (2), $[ZnL^{Cu}(H_2O)_2(MeOH)_2]_n$ (3), $[ML^{Cu}(H_2O)_4]_n$ (M = Mn (7), Fe (8)), and $\{[Cu(2,2'\text{-bpy})L^{Cu}]\cdot 3H_2O\}_n$ (9). Crystal structures of **2** and **3** have been previously reported,[9] and therefore, only bonding schemes are described to compare the structural features with those of other novel coordination polymers **4**−**10**. These compounds are structurally coordination 2-D network polymers, but they are different from each other in bonding modes as shown in Figure 4.

In **2**, the two 4-carboxylate groups of L^{Cu} act as unidentate coordination and bidentate semichelating ligands to bridge

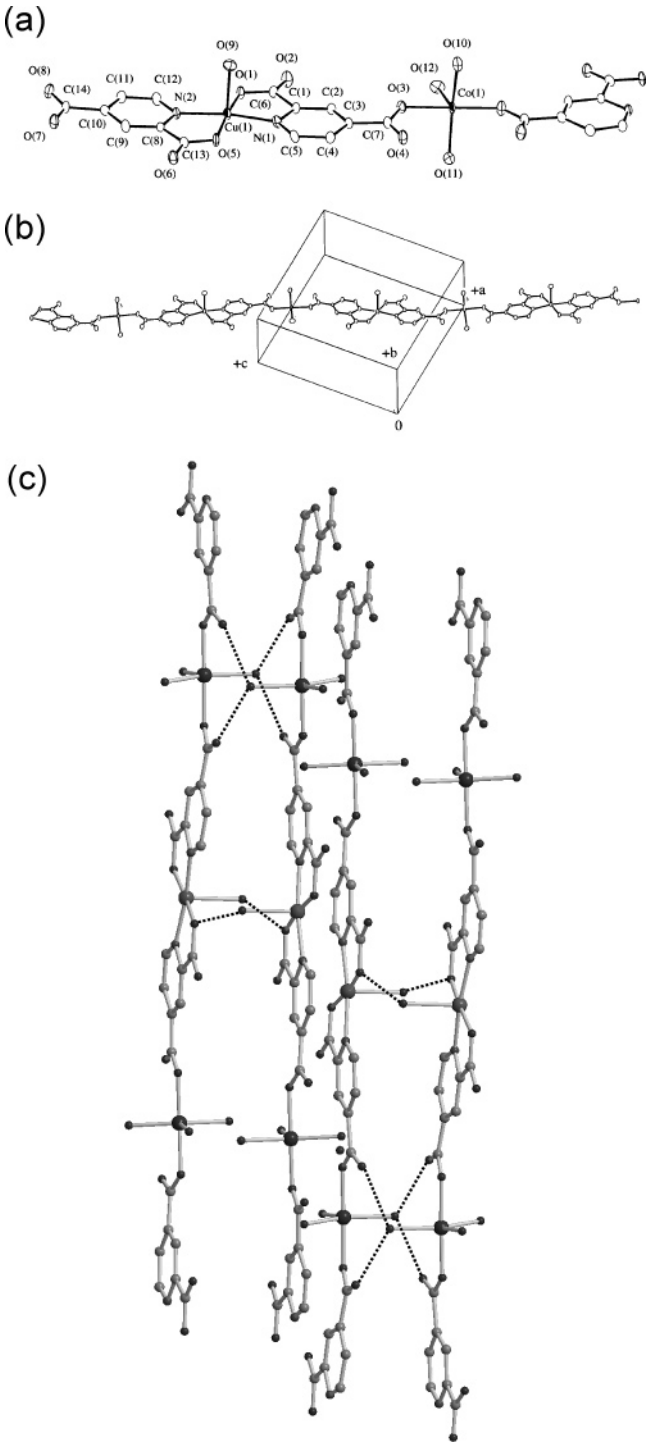

Figure 3. Structure of **4**. (a) ORTEP drawing around Cu^{II} and Co^{II} centers at the 30% probability level. (b) ORTEP view of the 1-D linear chain structure at the 30% probability level. (c) View of the hydrogen-bonding network among the 1-D chains. The dotted lines indicate hydrogen bonds. The guest H_2O molecules and hydrogen bonds between the chains and free H_2O molecules are omitted for clarity.

Zn^{II} ions, forming an undulated coordination 1-D chain. The chains are bound between Cu^{II} and Zn^{II} ions via a H_2O molecule, consequently forming a 2-D coordination sheet, which interacts with the neighboring sheets through hydrogen bonds between Zn-coordinated H_2O molecules and the oxygen atoms of 2- or 4-carboxylate groups. In **3**, the 4-carboxylate groups of L^{Cu} bridge Zn^{II} ions to form a

Table 3. Selected Bond Distances (Å) and Angles (deg) of **4**−**6**[a]

	4 (M = Co)	**5** (M = Cu(2))	**6** (M = Zn)
	Distances		
Cu(1)−O(1)	1.969(3)	1.964(2)	1.966(3)
Cu(1)−O(5)	1.944(3)	1.952(2)	1.945(3)
Cu(1)−O(9)	2.268(3)	2.267(3)	2.261(3)
Cu(1)−N(1)	1.974(3)	1.975(2)	1.980(3)
Cu(1)−N(2)	1.992(3)	1.992(2)	2.000(3)
M−O(3)	1.989(3)	1.942(2)	2.036(2)
M−O(7*)	1.960(3)	1.924(2)	1.992(3)
M−O(10)	2.032(3)	2.013(3)	2.068(3)
M−O(11)	1.981(3)	1.961(3)	2.032(3)
M−O(12)	2.155(3)	2.200(3)	2.029(3)
	Angles		
O(1)−Cu(1)−O(5)	173.3(1)	173.18(9)	173.3(1)
O(1)−Cu(1)−O(9)	93.6(1)	93.57(9)	93.5(1)
O(1)−Cu(1)−N(1)	82.5(1)	82.76(9)	82.8(1)
O(1)−Cu(1)−N(2)	100.1(1)	100.03(10)	100.4(1)
O(5)−Cu(1)−O(9)	92.1(1)	92.39(9)	92.1(1)
O(5)−Cu(1)−N(1)	93.8(1)	93.65(9)	93.3(1)
O(5)−Cu(1)−N(2)	82.8(1)	82.76(9)	82.7(1)
O(9)−Cu(1)−N(1)	92.7(1)	92.67(10)	92.4(1)
O(9)−Cu(1)−N(2)	94.7(1)	94.76(10)	94.9(1)
N(1)−Cu(1)−N(2)	172.0(1)	171.9(1)	171.8(1)
O(3)−M−O(7*)	178.2(1)	177.07(10)	176.0(1)
O(3)−M−O(10)	89.4(1)	89.83(10)	88.7(1)
O(3)−M−O(11)	88.5(1)	88.86(10)	87.0(1)
O(3)−M−O(12)	85.1(1)	84.95(9)	87.5(1)
O(7*)−M−O(10)	91.7(1)	91.2(1)	91.6(1)
O(7*)−M−O(11)	91.3(1)	91.3(1)	90.4(1)
O(7*)−M−O(12)	93.3(1)	92.19(9)	96.3(1)
O(10)−M−O(11)	152.4(1)	156.6(1)	144.2(1)
O(10)−M−O(12)	99.7(1)	97.79(10)	103.6(1)
O(11)−M−O(12)	107.6(1)	105.4(1)	111.7(1)

[a] Symmetry code: (*) $x - {}^1/_2, {}^1/_2 - y, z + 1$.

coordination 1-D chain. The chains are bound by weak coordination bonds between remaining oxygen atoms of the 4-carboxylate groups and the Cu^{II} centers of neighboring chains to form a 2-D coordination network (Cu−O = 2.883(3) Å). In analogy to **2**, each 2-D sheet is linked by hydrogen bonds between the coordinated H_2O molecules at the Zn^{II} centers and the oxygen atoms of 2-carboxylate. In both **2** and **3**, the 2-carboxylate groups are not involved in any coordination links as in the case of **4**−**6**.

In contrast to **2** and **3** and 1-D polymers **4**−**6**, the metalloligand L^{Cu} in **7** and **8** acts as a quasitetradentate bridge unit, where both 2- and 4-carboxylate groups are utilized to form a 2-D network. An ORTEP view around the metal centers of **7** is representatively shown in Figure 5a as **7** and **8** are isomorphous. Selected bond distances and angles of **7** and **8** are listed in Table 4. The Mn^{II} center is based on a distorted octahedral environment occupied by four H_2O molecules and two oxygen donors of 2-carboxylate groups of the metalloligands with a bond distance of Mn(1)−O(2) = 2.198(3) Å, forming an alternating zigzag 1-D chain (Figure 5b), where the intrachain Cu···Mn distance is ca. 5.15 Å. Since the metalloligand is axially and weakly occupied by two oxygen atoms supplied from 4-carboxylate groups of other symmetry-independent L^{Cu} species (Cu(1)−O(3) = 2.712(4) Å), **7** forms a coordination 2-D network, which is also supported by hydrogen bonds between the coordinated H_2O molecules at the Mn^{II} centers and the oxygen atoms of the 4-carboxylate groups (2.867(4) Å) as shown in Figure 5c and by $\pi-\pi$ interactions between pyridine rings of the 2,4-pydca^{2-} ligands (C···C = 3.4−3.5 Å, C···N = 3.4 Å). The shortest interchain Cu···Cu, Cu···Mn, and Mn···Mn distances are ca. 7.90, 8.01, and 7.90 Å, respectively. Each 2-D sheet is linked by hydrogen bonds between coordinated H_2O molecules at the Mn^{II} ions and the oxygen atoms of 4-carboxylate (the shortest hydrogen-bonding distance is 2.690(5) Å) (Figure 5d). The $\pi-\pi$ interactions between pyridine rings and carboxylate parts (C···O = 3.2−3.3 Å) assist an intersheet assembly. The shortest intersheet Cu···Mn distance is ca. 5.85 Å. For **8**, the intrachain Cu···Fe, interchain Cu···Cu, Cu···Fe, Fe···Fe, and intersheet Cu···Fe distances are ca. 5.09, 7.77, 7.81, 7.77, and 5.81 Å, respectively.

The metalloligand L^{Cu} in **9** also functions as a quasitetradentate bridge, but its coordination mode is slightly different from those of **7** and **8**. An ORTEP view around the Cu^{II} centers of **9** is shown in Figure 6a. Selected bond distances and angles are listed in Table 5. The metalloligands bridge another Cu^{II} (Cu(2)) metal complex building block

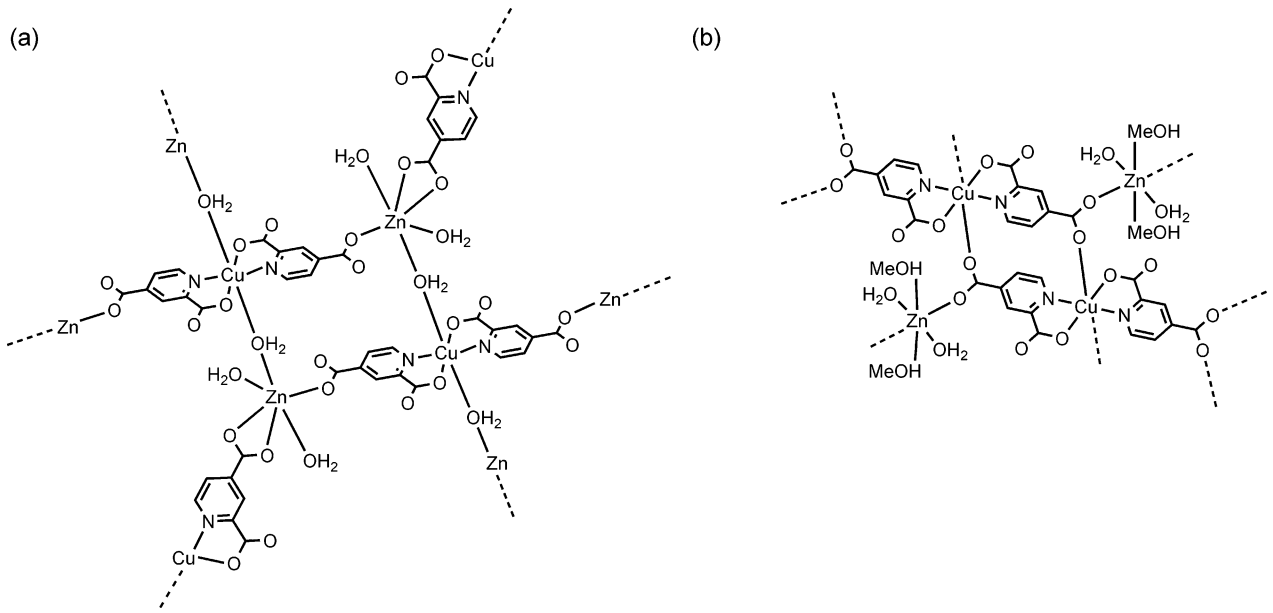

Figure 4. Schematic views of the L^{Cu} bonding modes of (a) **2** and (b) **3**.

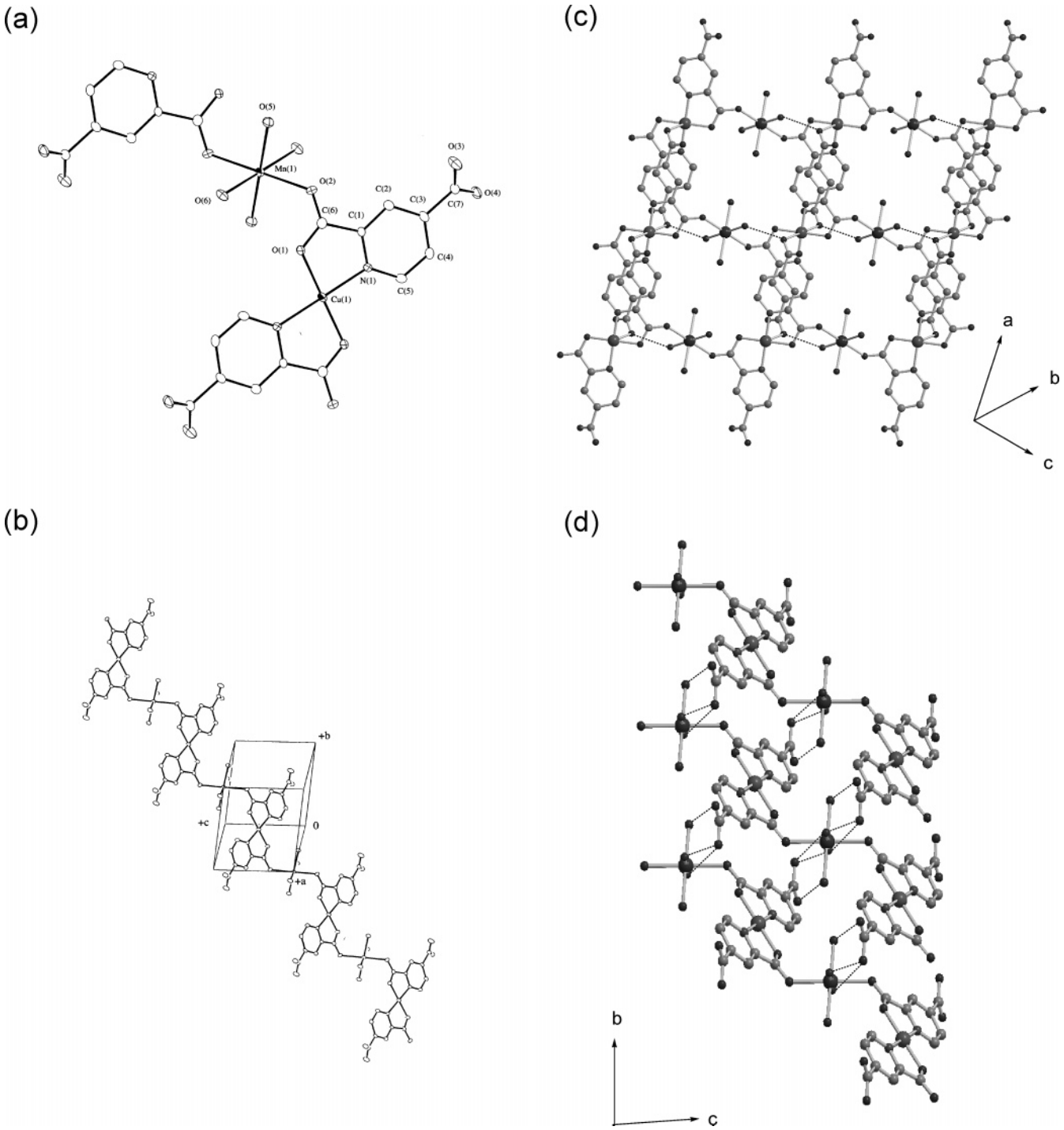

Figure 5. Structure of **7**. (a) ORTEP drawing around Cu^{II} and Mn^{II} centers at the 30% probability level. (b) ORTEP view of the 1-D zigzag chain structure at the 30% probability level. (c) View of the 2-D sheet structure. The dotted lines indicate intralayer hydrogen bonds. (d) View of the hydrogen-bonding network between the 2-D sheets along the *a*-axis. The dotted lines indicate interlayer hydrogen bonds.

with a 2,2′-bpy terminal ligand by 4-carboxylate groups to form a zigzag chain structure, where Cu(2) has a pentagonal geometry, and the bond distances with 4-carboxylate groups are Cu(2)−O(3) = 2.608(5) Å, Cu(2)−O(4) = 1.933(5) Å, and Cu(2)−O(8) = 1.924(4) Å. The axial positions of the metalloligand moiety are occupied by weak coordination of two oxygen donors of 2-carboxylate groups of the nearest-neighboring L^{Cu} with an average bond distance of 2.760 Å, so that **9** is a 2-D coordination polymer with an undulated network (Figure 6b). The 2-D undulated network is stabilized by $\pi-\pi$ interactions between pyridine rings of the 2,2′-bpy ligands (C···C = 3.4−3.6 Å, C···N = 3.6 Å) and between pyridinedicarboxylate parts (C···C = 3.3−3.4 Å, C···O = 3.0−3.5 Å). The interchain Cu(1)···Cu(1) distance is ca. 5.17 Å. The shortest intersheet Cu···Cu bond distance (Cu(2)···Cu(2)) is ca. 7.91 Å. No bonding interaction was observed between the 2-D undulated sheets.

Crystal Structure of 3-D Polymer $[Ag_2L^{Cu}]_n$ (10). Figure 7a shows an ORTEP view around the metal centers of **10**. Selected bond distances and angles are listed in Table 6. The

Table 4. Selected Bond Distances (Å) and Angles (deg) of **7** and **8**[a]

	7 (M = Mn)	**8** (M = Fe)
Distances		
Cu(1)−O(1)	1.936(3)	1.927(2)
Cu(1)−O(4*)	2.712(4)	2.665(3)
Cu(1)−N(1)	1.995(3)	1.963(3)
M(1)−O(2)	2.198(3)	2.135(2)
M(1)−O(5)	2.217(3)	2.166(3)
M(1)−O(6)	2.185(3)	2.087(2)
Angles		
O(1)−Cu(1)−O(1**)	180.0	180.0
O(1)−Cu(1)−O(4*)	94.4(1)	94.55(10)
O(1)−Cu(1)−N(1)	84.5(1)	83.9(1)
O(4*)−Cu(1)−O(4***)	180.0	180.0
O(4*)−Cu(1)−N(1*)	91.5(1)	90.65(10)
N(1)−Cu(1)−N(1**)	180.0	180.0
O(2)−M(1)−O(2****)	180.0	180.0
O(2)−M(1)−O(5)	84.2(1)	83.89(10)
O(2)−M(1)−O(6)	97.5(1)	96.12(10)
O(5)−M(1)−O(5****)	180.0	180.0
O(5)−M(1)−O(6)	91.1(1)	90.53(10)
O(6)−M(1)−O(6****)	180.0	180.0

[a] Symmetry code: (*) $x + 1, y, z$; (**) $2 - x, 1 - y, 1 - z$; (***) $1 - x, 1 - y, 1 - z$; (****) $2 - x, 2 - y, 2 - z$.

metalloligand L^{Cu} acts as a multidentate bridge. The 4-carboxylate groups of the metalloligand bridge a dimer of Ag^{I} with an average Ag−O bond distance of 2.214 Å to form a 1-D arrangement, where the Ag−Ag bond distance is 2.8822(5) Å, slightly shorter than that in metallic silver (2.89 Å), indicative of a weak metal−metal interaction.[10] The 2-carboxylate groups coordinate to the dimer of Ag^{I} with a bond distance of Ag(1)−O(2) = 2.415(3) Å, consequently forming a 2-D network shown in Figure 7b. The 4- and 2-carboxylate groups of the metalloligand also weakly coordinate to the Ag ions with a bond distance of Ag(1)−O(3) = 2.713(3) Å, and the Cu^{II} centers of the metalloligands with a bond distance of Cu(1)−O(2) = 2.795(3) Å, respectively, finally constructing a 3-D network (Figure 7c), where the Cu^{II} center has an elongated octahedral geometry. The assembly of each 2-D sheet is also supported by $\pi-\pi$ interactions between pyridinedicarboxylate parts (C···C = 3.3−3.5 Å, C···O = 3.2−3.5 Å, N···O = 3.2 Å). The shortest Cu···Cu distance in the 2-D sheet is 10.22 Å (the Cu···Cu distance in the 1-D chain direction is 16.60 Å). The shortest Cu···Cu distance between neighboring 2-D sheets is 5.12 Å.

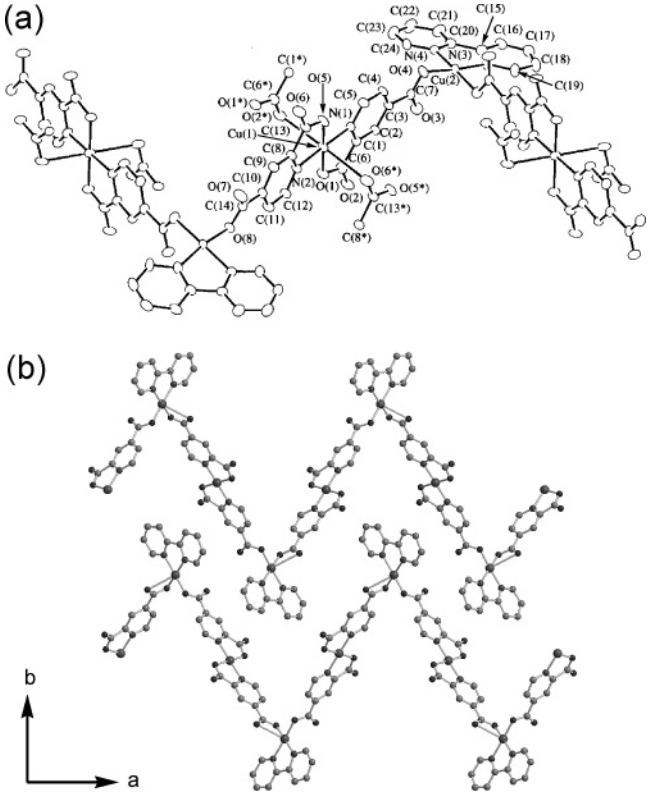

Figure 6. Structure of **9**. (a) ORTEP drawing of the 1-D zigzag chain at the 30% probability level. (b) View of the 2-D undulated sheets along the *c*-axis. The guest H_2O molecules are omitted for clarity.

Metalloligand with Multicoordination Ability: Selective Bond Formation of Coordination Networks. To date, a large number of heterometallic Cu−M coordination polymers bridged by organic ligands (Mn−Cu,[7d,g−m,8a−d,f−h,11] Fe−Cu,[12] Co−Cu,[7b,f,8e] Zn−Cu,[7e,13] and Ag−Cu[7o,14]) have been reported. Herein we succeeded in systematic syntheses of a series of mixed-metallic coordination polymers by utilizing the metalloligand L^{Cu} with multicoordination ability. As mentioned above, L^{Cu} is able to have six characteristic bonding modes depending on metal ions as shown in Chart 2. All the coordination polymers are classified on the basis of the coordination modes: (i) bridging number of the

Table 5. Selected Bond Distances (Å) and Angles (deg) for **9**[a]

Distances					
Cu(1)−O(1)	1.959(5)	Cu(1)−O(2*)	2.713(6)	Cu(1)−O(5)	1.929(5)
Cu(1)−O(6**)	2.806(6)	Cu(1)−N(1)	1.971(5)	Cu(1)−N(2)	1.955(5)
Cu(2)−O(3)	2.608(5)	Cu(2)−O(4)	1.933(5)	Cu(2)−O(8***)	1.924(4)
Cu(2)−N(3)	1.995(6)	Cu(2)−N(4)	1.974(5)		
Angles					
O(1)−Cu(1)−O(2*)	95.6(2)	O(1)−Cu(1)−O(5)	179.3(2)		
O(1)−Cu(1)−O(6**)	84.0(2)	O(1)−Cu(1)−N(1)	83.9(2)		
O(1)−Cu(1)−N(2)	95.1(2)	O(2*)−Cu(1)−O(5)	84.8(2)		
O(2*)−Cu(1)−O(6**)	178.7(1)	O(2*)−Cu(1)−N(1)	92.1(2)		
O(2*)−Cu(1)−N(2)	90.8(2)	O(5)−Cu(1)−O(6**)	95.6(2)		
O(5)−Cu(1)−N(1)	96.7(2)	O(5)−Cu(1)−N(2)	84.3(2)		
O(6**)−Cu(1)−N(1)	89.2(2)	O(6**)−Cu(1)−N(2)	88.0(2)		
N(1)−Cu(1)−N(2)	177.1(3)	O(3)−Cu(2)−O(4)	55.7(2)		
O(3)−Cu(2)−O(8***)	88.6(2)	O(3)−Cu(2)−N(3)	127.7(2)		
O(3)−Cu(2)−N(4)	88.4(2)	O(4)−Cu(2)−O(8***)	90.7(2)		
O(4)−Cu(2)−N(3)	175.1(3)	O(4)−Cu(2)−N(4)	95.1(2)		
O(8***)−Cu(2)−N(3)	92.8(2)	O(8***)−Cu(2)−N(4)	170.4(3)		
N(3)−Cu(2)−N(4)	81.9(2)				

[a] Symmetry code: (*) $x, y, z - 1$; (**) $x, y, z + 1$; (***) $^1/_4 + x, ^1/_4 - y, ^5/_4 + z$.

Table 6. Selected Bond Distances (Å) and Angles (deg) for **10**[a]

Distances			
Ag(1)−Ag(1*)	2.8822(5)	Ag(1)−O(2**)	2.415(3)
Ag(1)−O(3)	2.211(3)	Ag(1)−O(4***)	2.713(3)
Ag(1)−O(4*)	2.216(3)	Cu(1)−O(1)	1.945(2)
Cu(1)−O(2****)	2.795(3)	Cu(1)−N(1)	1.949(3)
Angles			
Ag(1*)−Ag(1)−O(2**)	154.07(6)	Ag(1*)−Ag(1)−O(3)	76.56(7)
Ag(1*)−Ag(1)−O(4***)	115.71(6)	Ag(1*)−Ag(1)−O(4*)	86.60(7)
O(2**)−Ag(1)−O(3)	83.92(9)	O(2**)−Ag(1)−O(4***)	82.24(9)
O(2**)−Ag(1)−O(4*)	112.66(10)	O(3)−Ag(1)−O(4***)	94.16(10)
O(3)−Ag(1)−O(4*)	163.1(1)	O(4***)−Ag(1)−O(4*)	91.61(9)
O(1)−Cu(1)−O(1****)	180.0	O(1)−Cu(1)−O(2*****)	97.58(9)
O(1)−Cu(1)−N(1)	84.4(1)	O(2*****)−Cu(1)−O(2******)	180.0
O(2*****)−Cu(1)−N(1)	82.77(9)	N(1)−Cu(1)−N(1****)	180.0

[a] Symmetry Code: (*) $2-x, 1-y, -z$; (**) $1-x, -y, -z$; (***) $x, y, 1+z$; (****) $-x, -y, -2-z$; (*****) $x, y, z-1$; (******) $-x, -y, -1-z$.

metalloligand L^{Cu}, (ii) role of the Lewis-acidic Cu^{II} site, and (iii) selective bond formation for first-period transition metal ions.

First, the six coordination modes are distinguishable in terms of (i) bridging number of L^{Cu}: this is two for **4**−**6**, three for **2**, four for **3** and **7**−**8**, five for **9**, and ten for **10**. Second, when the 2-carboxylate groups are coordinated to secondary metal ions, the axial sites of the central Cu^{II} ion are commonly occupied by anionic 2- or 4-carboxylate oxygen atoms of another metalloligands, affording high coordination numbers. This structural aspect is seen in the case of **7**−**10**, characteristic of a regulation effect by the central Cu^{II} ion of the metalloligand. Namely, Lewis acidity of the Cu^{II} sites of the metalloligand is closely related to Lewis basicity of the 2-carboxylate groups. The case of **3** looks like an exceptional case; despite the 2-carboxylate sites being coordination-free, the central Cu^{II} ion has an axial coordination mode with the 4-carboxylate groups. However, considering the fact that the Cu−O(4-carboxylate) bond of **3** is very long with 2.883(3) Å compared with those of **7**−**10** (Cu−O = 2.665−2.806 Å), **3** is not in this case. These results reveal that this metalloligand L^{Cu} can flexibly change its

Chart 2

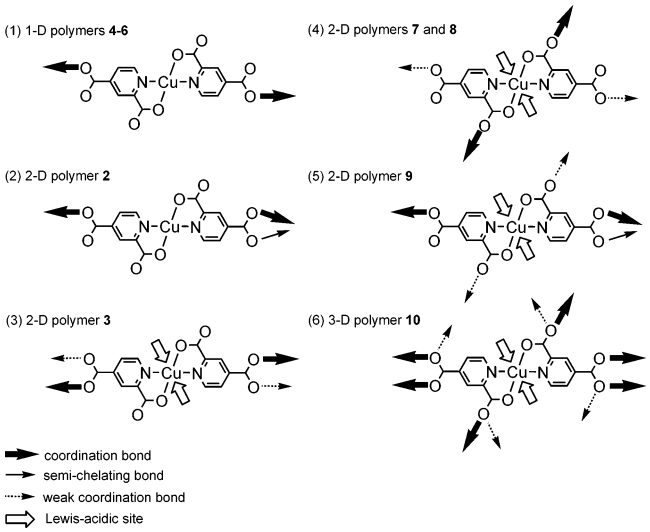

coordination affinity for acting as both coordination-donor and -acceptor with the aid of second metal units employed. Third, L^{Cu} selectively binds for divalent ions of the first-period transition metal series (Mn^{II}, Fe^{II}, Co^{II}, Cu^{II}, and Zn^{II}):[15] as Cu^{II} and Zn^{II} ions, the 4-carboxylate groups are selectively bound to the present metal ions, and as Mn^{II} and Fe^{II} ions, the 2-carboxylate groups coordinate selectively to the present metal ions.[16] It is well-known that the stabilities of corresponding complexes of such metal series, irrespective of the particular ligand involved, usually vary in the Irving−Williams order,[17] $Mn^{II} < Fe^{II} < Co^{II} < Ni^{II} < Cu^{II} > Zn^{II}$, which is related to the electrostatic and covalent interactions, namely, the reciprocal of the ionic radius and the second ionization potential, both of which increase monotonically throughout the series from Mn to Cu. Although Zn ion has also a higher ionization potential and a smaller radius than those of Ni and Co, an orbital stabilization, which generally increases in Cu complexes, makes the order of Cu and Zn reversed.[17] In the case of the metalloligand L^{Cu}, the 4-carboxylate groups have a stronger coordination ability and

(10) Wu, D.-D.; Mak, T. C. W. *J. Chem. Soc., Dalton Trans.* **1995**, 2671−2678.
(11) (a) Gleizes, A.; Verdaguer, M. *J. Am. Chem. Soc.* **1981**, *103*, 7373−7374. (b) Solans, X.; Font-Altaba, M.; Oliva, J.; Herrera, J. *Acta Crystallogr.* **1983**, *C39*, 435−438. (c) Kim, J.; Lim, J. M.; Choi, Y.-K.; Do, Y. *Angew. Chem., Int. Ed. Engl.* **1996**, *35*, 998−1000.
(12) (a) Morpurgo, G. O.; Mosini, V.; Porta, P.; Dessy, G.; Fares, V. *J. Chem. Soc., Dalton Trans.* **1980**, 1272−1276. (b) Morpurgo, G. O.; Mosini, V.; Porta, P.; Dessy, G.; Fares, V. *J. Chem. Soc., Dalton Trans.* **1981**, 111−117. (c) Kou, H.-Z.; Liao, D.-Z.; Cheng, P.; Jiang, Z.-H.; Yan, S.-P.; Wang, G.-L.; Yao, X.-K.; Wang, H.-G. *J. Chem. Soc., Dalton Trans.* **1997**, 1503−1506. (d) Kou, H.-Z.; Wang, H.-M.; Liao, D.-Z.; Cheng, P.; Jiang, Z.-H.; Yan, S.-P.; Huang, X.-Y.; Wang, G.-L. *Aust. J. Chem.* **1998**, *51*, 661. (e) Zou, J.; Hu, X.; Duan, C.; Xu, Z.; You, X. *Transition Met. Chem.* **1998**, *23*, 477. (f) Gomez-Romero, P.; Jameson, G. B.; Borras-Almenar, J. J.; Escriva, E.; Coronado, E.; Beltran, D. *J. Chem. Soc., Dalton Trans.* **1988**, 2747−2751. (g) Morgenstern-Badarau, I.; Laroque, D.; Bill, E.; Winkler, H.; Trautwein, A. X.; Robert, F.; Jeannin, Y. *Inorg. Chem.* **1991**, *30*, 3180−3188. (h) Chen, Z. N.; Wang, J. L.; Qui, J.; Miao, F. M.; Tang, W. X. *Inorg. Chem.* **1995**, *34*, 2255−2257.
(13) Ogata, T.; Taga, T.; Osaki, K. *Bull. Chem. Soc. Jpn.* **1977**, *50*, 1680−1682.
(14) (a) Dong, Y.-B.; Smith, M. D.; zur Loye, H.-C. *Solid State Chem.* **2000**, *2*, 335−342. (b) Brouca-Cabarrecq, C.; Marrot, B.; Mosset, A. *Acta Crystallogr.* **1996**, *C52*, 1903−1906. (c) Krautscheid, H.; Emig, N.; Klaassen, N.; Seringer, P. *J. Chem. Soc., Dalton Trans.* **1998**, 3071−3077.
(15) Although we tried to attempt a reaction of the L^{Cu} with a Ni^{II} ion, a desired mixed-metallic compound was not obtained.
(16) We did not consider weak metal−carboxylate bonds in the discussion about the bond selectivity of L^{Cu}.
(17) Irving, H.; Williams, R. J. P. *J. Chem. Soc.* **1953**, 3192−3210.

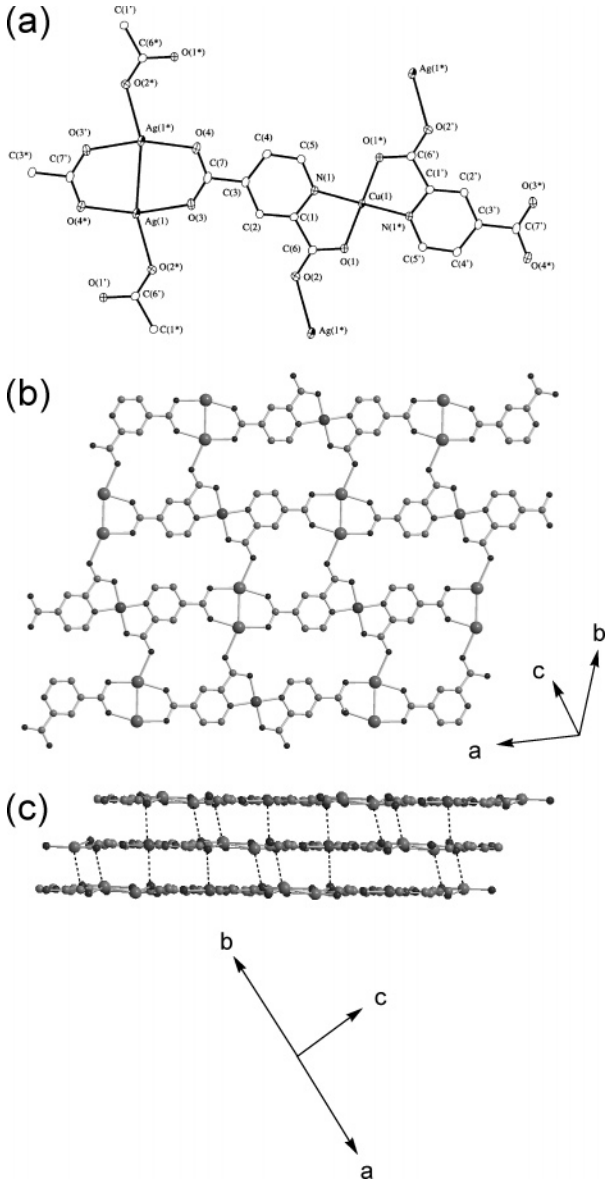

Figure 7. Structure of **10**. (a) ORTEP drawing around Cu^{II} and Ag^{I} centers at the 30% probability level. (b and c) View of (b) the 2-D sheet structure and (c) the 3-D network. The dotted lines indicate interlayer weak coordination bonds.

electrostatic effect than the 2-carboxylate groups that coordinate to the Lewis-acidic, cationic Cu^{II} center. Therefore, the bonding selectivity of the carboxylate groups could be anticipated for divalent ions of the first-period transition metal series: Co^{II}, Cu^{II}, and Zn^{II} ions form stabler bonds with 4-carboxylate parts than 2-carboxylate ones while Mn^{II} and Fe^{II} ions prefer 2-carboxylate bridges more than 4-carboxylate ones. The trend obtained in the case of L^{Cu} is not explained at present. As far as the experimental results, we succeeded in selective bond formation by utilizing the different coordination groups (sites) of the metalloligand L^{Cu}, i.e., multicoordination ability. Thus, the metalloligand L^{Cu} may be a candidate for useful building units for rational construction of novel coordination polymers having mixed metals and various dimensions. This selective bond formation played an important role in control of magnetic properties in the compounds.

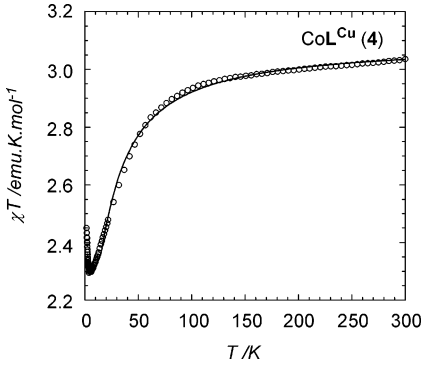

Figure 8. Temperature dependence of the χT product at 1 kOe measured on a polycrystalline sample of **4**. The solid line represents a fitting performed using alternating classical spin model (see text) in the temperature range 15−300 K.

Magnetic Properties. In this section, the magnetic properties are discussed on the basis of the bridging mode between metal centers. The difference of the bridging mode between the Cu^{II} ion of L^{Cu} and second metal units influenced magnetic properties of the compounds. Compounds **4**, **5**, and **9**, which have the 4-carboxypyridinate bridge between magnetic centers, show weak antiferromagnetic interaction, while **7** and **8** with the carboxylate bridges, to the contrary, exhibit ferromagnetic behavior. Compounds **6** and **10** could be paramagnetic because of no relevant exchange interaction between Cu^{II} ions via diamagnetic Zn and Ag_2 moieties, respectively, but exhibit weak interchain or interlayer antiferromagnetic interaction. Thus, these compounds can be classified into three groups on the magnetic properties.

Direct current magnetic measurements were performed on polycrystalline samples of **4**−**10** between 300 and 1.82 K under an external field of 1 kOe. For **4**, **5**, and **9** (first group), the temperature dependence of $1/\chi$ between 300 and 50 K obeys roughly the Curie−Weiss law with $C = 3.08$ emu·K·mol^{-1} and $\theta = -5.32$ K for **4**, $C = 0.94$ emu·K·mol^{-1} and $\theta = 0.79$ K for **5**, and $C = 0.83$ emu·K·mol^{-1} and $\theta = -0.78$ K for **9**. Each Curie constant is in good agreement with the expected value of 2.25 emu·K·mol^{-1} for **4** (Cu^{II}−Co^{II}), and 0.75 emu·K·mol^{-1} for **5** and **9** (Cu^{II}−Cu^{II}), assuming an average g value of 2.00 (slight large values should be according to g values larger than 2.00). The small values of the Weiss constant indicate a weak interaction between the magnetic centers. Indeed, the χT behavior as a function of temperature is nearly flat at the temperature range 300−100 K (Figure 8 for **4** and Figure 9 for **5** and **9**). Considering long metal-to-metal distance via the 4-carboxypyridinate bridge, it can be easily understood that the corresponding exchange interaction is relatively weak. (In the case of **9**, although the carboxylate bridge between the Cu(1) ions also exists, the magnetic interaction between them can be neglected due to the weak bridge (av 2.760 Å).) Nevertheless, compound **4** may be not in this case. As realized from their structures, these compounds can be magnetically assumed as 1-D chain. To estimate intrachain magnetic exchange coupling (via 4-carboxypyridinate bridge), the magnetic susceptibility at the temperature range 300−5 K (300−15 K for **4**) was simulated by using an alternating

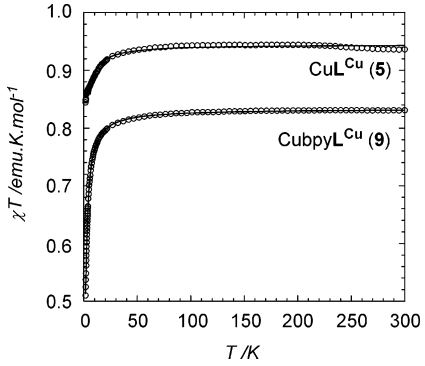

Figure 9. Temperature dependence of the χT product at 1 kOe measured on polycrystalline samples of **5** (upper) and **9** (bottom). The solid line represents a fitting performed using alternating classical spin model (see text) in the temperature range 5−300 K.

Table 7. Magnetic Parameters Obtained from Simulations on Magnetic Susceptibilities

compd	g_M	g_{Cu}	J/k_B[a] (K)	zJ'/k_B[b] (K)
4[c]	2.40 (M = Co)	2.05	−4.05	
5[c]	2.24 (M = Cu)	2.24	−0.57	
6[d]		2.19		−0.17
7[c]	2.00 (M = Mn)	2.10	0.69	
8[c]	2.12 (M = Fe)	2.25	0.71	
9[c]	2.11 (M = Cu)	2.11	−0.89	
10[d]		2.12		−1.51

[a] From the simulation using the alternating classical spin model. [b] From the simulation with the mean-field approximation treatment. [c] Using the alternating classical spin model. [d] Treated by the mean-field approximation.

chain model of classical spins reported by Drillon et al.,[18] based on the following Hamiltonian:

$$H = -2J\sum_{i=1}^{N} S_i \cdot S_{i+1} \qquad (1)$$

where S_i is the current spin vector at the ith site, and $S_{2i-1} = S_{Cu}$ and $S_{2i} = S_{Co}$ for **4**, $S_{2i} = S_{Cu}$ for **5** and **9**. The obtained best sets for the compounds are summarized in Table 7. It is well-known that Co^{II} ion with an octahedral surrounding, generally, has a strong spin−orbit coupling in its ground state $^4T_{1g}$. In the case of **4**, the coordination geometry around Co^{II} ion is very close to square-pyramid with pentacoordination (D_{4h}) which would also experience such an effect.[3a] However, the simulation was approximately performed by neglecting its effect.[19] For all these compounds, the contribution of interchain interaction was also neglected in the fitting above 5 K, because the interchain interaction (Cu(1)···Cu(1) interaction) is expected to be very weak as ~ -0.1 K as observed in **6** (vide infra). However, the interchain Co···Co distance (4.43 Å) in **4** is shorter than the interchain Cu(1)···Cu(1) distance (5.34 Å) in **6** as described in the structural section. Therefore, the origin for the relative large exchange coupling in **4** can be considered in two possibilities: (i) ferrimagnetic spin arrangement in a chain as simulated above, and (ii) the contribution of the interchain Co···Co antiferromagnetic interaction and intrachain Co···Cu antiferromagnetic interaction with spin-canting (i.e., 2-D antiferromagnetic coupling with spin-canting). Indeed, both assumptions are able to yield a χT minimum (2.30 emu·K·mol^{-1} at 5.3 K) and an abrupt increase in the low-temperature region (Figure 8), but we could, unfortunately, not define the actual exchange process.

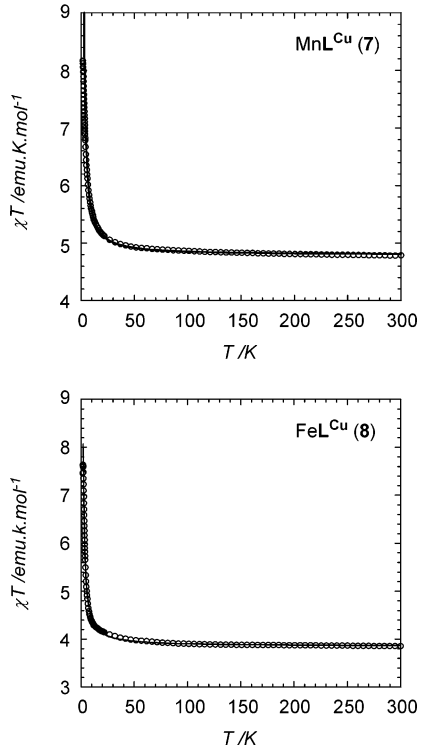

Figure 10. Temperature dependence of the χT product at 1 kOe measured on polycrystalline samples of **7** (upper) and **8** (bottom). The solid line represents a fitting performed using alternating classical spin model (see text) in the temperature range 7−300 K.

For **7** and **8** (second group), temperature dependence of $1/\chi$ between 300 and 50 K obeys roughly the Curie−Weiss law with $C = 4.75$ emu·K·mol^{-1} and $\theta = 2.28$ K for **7** and $C = 3.84$ emu·K·mol^{-1} and $\theta = 1.82$ K for **8**. The obtained Curie constant is in good agreement with the expected value of 4.75 emu·K·mol^{-1} for **7** (Cu^{II}−Mn^{II}) and 3.38 emu·K·mol^{-1} for **8** (Cu^{II}−Fe^{II}) ($g_{av} = 2.0$). Here, we should give attention to the obtained positive Weiss constants, ferromagnetic interaction between the magnetic centers being dominant. As mentioned already, **7** and **8** have a 2-D network structure consisting of two bridging modes of 4-carboxypyridinate and carboxylate bridges (see structural description). Considering the small antiferromagnetic contribution mediated by 4-carboxypyridinate as realized from the results of the first group in addition to the weak 4-carboxypyridinate bridge (2.712(4) and 2.665(3) Å for **7** and **8**, respectively), the positive Weiss constant obtained in the high temperature region reflects principally the magnetic interaction via the 2-carboxylate pathway. Considering this matter, **7** and **8** can therefore be assumed magnetically to be a quasi-1-D alternating chain bridged by a carboxylate group. Figure 10 shows plots of the temperature dependence of χT of **7** and **8**. Both magnetic behaviors are very similar to each other. With decreasing temperature, the χT value at 300 K, 4.79 emu·K·mol^{-1} for **7** and 3.86 emu·K·mol^{-1} for **8**, gradually increases followed

(18) Drillon, M.; Coronado, E.; Beltran, D.; Georges, R. *Chem. Phys.* **1983**, *79*, 449−453.
(19) The effect of spin−orbit coupling for Co^{II} ion may be oversimulated as the g value for Co^{II} ion. See Table 7.

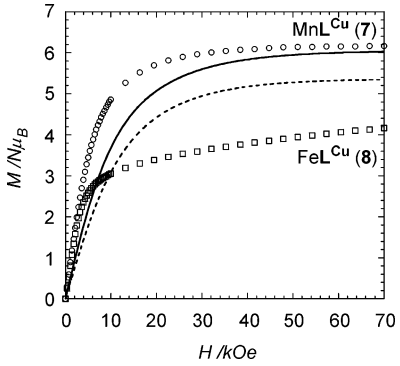

Figure 11. Field dependence of the magnetization at 1.82 K measured on polycrystalline samples of **7** and **8**. The solid and dashed lines represent simulation curves with $S = {}^5/_2 + {}^1/_2$ and $S = 2 + {}^1/_2$ (paramagnetic system with no interaction), respectively, where the g values in Table 8 that were experimentally obtained were used in the simulations.

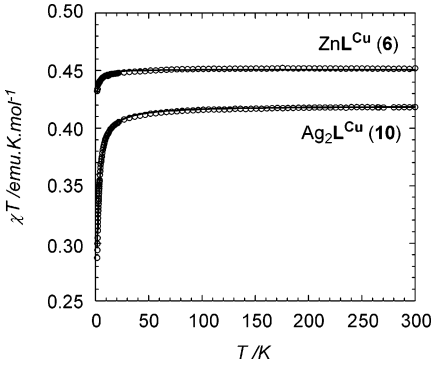

Figure 12. Temperature dependence of the χT product at 1 kOe measured on polycrystalline samples of **6** (upper) and **10** (bottom). The solid line represents a fitting performed by the mean-field approximation (see text) in the temperature range 5−300 K.

by an abrupt increase to reach a maximum of 8.17 emu·K·mol^{-1} at 1.8 K and 7.64 emu·K·mol^{-1} at 2.0 K, respectively. With further decreasing temperature, for **8** it sharply decreases to 7.46 emu·K·mol^{-1} at 1.8 K. The observation of the abrupt increase of χT certainly supports ferromagnetic arrangement of the alternating bimetallic spins mediated by the carboxylate pathway. Assuming a 1-D magnetic chain via the carboxylate group, the magnetic susceptibility in the temperature range 300−7 K was simulated by using the alternating chain model of classical spins (eq 1) as well as the first group, where $S_{2i-1} = S_{Cu}$ and $S_{2i} = S_{Mn}$ or $S_{2i} = S_{Fe}$. The obtained best sets are summarized in Table 7.

The ferromagnetic arrangement can be also confirmed in field dependence of magnetization measured at 1.82 K (Figure 11). The solid and dashed curves in the figure were represented by Brillouin functions with the sets of paramagnetic centers, $S = {}^5/_2$ ($g = 2.00$) + ${}^1/_2$ ($g = 2.10$) and $S = 2$ ($g = 2.12$) + ${}^1/_2$ ($g = 2.25$), respectively (the g values correspond to the experimental values obtained from the best-fitting of χT (see Table 8)). The magnetization rapidly increases at low fields beyond the corresponding Brillouin function's curves, then gradually increases up to 7 T. The magnetization of **7** and **8** at 7 T is 6.2 and 4.2 μ_B, respectively, indicating their ferromagnetic arrangements between the magnetic centers. The overvalue of **7** against the expected value 6 μ_B as $g = 2.00$ should be due to the slightly large g value arising from the Cu^{II} ion ($g_{Cu} = 2.10$ derived from the fitting of the susceptibility). On the other hand, the considerably small value of **8**, as the expected value is 5 μ_B with $g = 2.00$, could be due to the effect of zero-field splitting of Fe^{II} ion.

Compounds **6** and **10** (third group) can be assumed to be paramagnetic ($C = 0.45$ emu·K·mol^{-1} and $\theta = -0.11$ K for **6**, and $C = 0.42$ emu·K·mol^{-1} and $\theta = -0.90$ K for **10**

Table 8. Crystallographic Data for [Cu(2,4-pydcaH)$_2$(H$_2$O)$_2$] (**1**·2H), (Et$_3$NH)$_2$[Cu(2,4-pydca)$_2$(H$_2$O)] (**1**·2Et$_3$NH), {[CoL^{Cu}(H$_2$O)$_4$]·**2**H$_2$O}$_n$ (**4**), {[CuL^{Cu}(H$_2$O)$_4$]·**2**H$_2$O}$_n$ (**5**), {[ZnL^{Cu}(H$_2$O)$_4$]·**2**H$_2$O}$_n$ (**6**), [MnL^{Cu}(H$_2$O)$_4$]$_n$ (**7**), [FeL^{Cu}(H$_2$O)$_4$]$_n$ (**8**), {[Cu(2,2′-bpy)L^{Cu}]·**3**H$_2$O}$_n$ (**9**), and [Ag$_2$L^{Cu}]$_n$ (**10**)

	1·2H	**1**·2Et$_3$NH	**4**	**5**	**6**	**7**	**8**	**9**	**10**
formula	$C_{14}H_{12}N_2CuO_{10}$	$C_{26}H_{40}N_4CuO_9$	$C_{14}H_{18}N_2CoCuO_{14}$	$C_{14}H_{18}N_2Cu_2O_{14}$	$C_{14}H_{18}N_2CuZnO_{14}$	$C_{14}H_{14}N_2CuMnO_{12}$	$C_{14}H_{12}N_2CuFeO_{12}$	$C_{24}H_{20}N_4Cu_2O_{11}$	$C_{14}H_6N_2Ag_2CuO_8$
fw	431.80	616.17	560.78	565.39	567.23	520.75	521.66	667.53	609.49
lattice	triclinic	monoclinic	monoclinic	monoclinic	monoclinic	triclinic	triclinic	orthorhombic	triclinic
a, Å	10.146(6)	18.546(3)	14.7281(9)	14.683(2)	14.779(2)	7.898(1)	7.7656(5)	35.954(2)	8.7317(7)
b, Å	11.319(6)	10.511(2)	8.3905(4)	8.398(1)	8.364(2)	8.005(1)	7.9258(6)	56.323(2)	8.7642(6)
c, Å	7.218(3)	15.050(2)	15.471(1)	15.4555(2)	15.4923(3)	7.580(1)	7.5144(5)	5.1710(2)	5.1250(5)
α, deg	97.41(4)					97.325(4)	97.499(4)		93.678(5)
β, deg	94.74(4)	95.404(4)	93.643(2)	93.0221(4)	93.8722(5)	90.874(7)	91.663(3)		99.508(3)
γ, deg	73.69(5)					112.07(1)	112.495(4)		108.496(2)
V, Å^3	788.0(7)	2920.9(8)	1907.9(2)	1903.2(2)	1910.7(3)	439.4(1)	422.08(5)	10471.4(8)	363.97(5)
space group	*P*$\bar{1}$ (No.2)	*C*2/*c* (No.15)	*P*2$_1$/*a* (No.14)	*P*2$_1$/*a* (No.14)	*P*2$_1$/*a* (No.14)	*P*$\bar{1}$ (No. 2)	*P*$\bar{1}$ (No.2)	*Fdd2* (No.43)	*P*$\bar{1}$ (No.2)
Z	2	4	4	4	4	1	1	16	1
ρ(calcd), g cm^{-3}	1.820	1.401	1.952	1.973	1.972	1.968	2.052	1.694	2.780
F(000)	438.00	1300.00	1136.00	1144.00	1148.00	262.00	263.00	5408.00	291.00
μ(Mo Kα), cm^{-1}	14.50	8.05	20.67	23.17	24.51	20.02	21.95	16.94	41.59
diffractometer	AFC7R	RAXIS-RAPID	RAXIS-RAPID	CCD	CCD	RAXIS-RAPID	RAXIS-RAPID	RAXIS-RAPID	RAXIS-RAPID
radiation (*λ*, Å)	0.71069	0.71069	0.71069	0.71069	0.71069	0.71069	0.71609	0.71069	0.71069
temp, °C	25	25	25	25	25	25	25	-40	25
R ($I > 2.00\sigma(I)$)[a]	0.040	0.036	0.041	0.037	0.042	0.047	0.039	0.044	0.029
R_w(all data)[b]	0.064	0.054	0.059	0.066	0.065	0.062	0.059	0.058	0.041
no. observations	3593 (all data)	3279 (all data)	3983 (all data)	4021 (all data)	3903 (all data)	1715 (all data)	1764 (all data)	3238 (all data)	1562 (all data)
no. variables	244	182	289	289	289	139	139	371	124

[a] $R = \sum||F_o| - |F_c||/\sum|F_o|$. [b] $R_w = [\sum w(|F_o| - |F_c|)^2/\sum wF_o^2]^{1/2}$.

in the temperature range 50−300 K). This is because of connecting diamagnetic centers, i.e., Zn^{II} ion for **6** and $[Ag_2]^{II}$ unit for **10**, with Cu^{II} paramagnetic centers via 4-carboxypyridinate and both carboxylate and 4-carboxypyridinate, respectively. Figure 12 shows the temperature dependence of χT of **6** and **10**. The χT values of 0.45 emu·K·mol^{-1} for **6** and 0.42 emu·K·mol^{-1} for **10** at 300 K are almost constant above 50 K, and then gradually decrease to 0.43 emu·K·mol^{-1} for **6** and 0.29 emu·K·mol^{-1} for **10** at 1.8 K. The decrease could be due to interchain or interlayer antiferromagnetic interaction between Cu^{II} ions. Note that the intrachain or intralayer Cu···Cu distance is significantly longer than the interchain or interlayer one. With a desire to estimate this interaction, the mean-field approximation was treated to a paramagnetic model with an $S = {}^1/_2$ ($\chi_{Cu} = Ng_{Cu}{}^2\mu_B{}^2/4kT$):

$$\chi = \frac{\chi_{Cu}}{1 - \dfrac{2zJ'}{Ng_{Cu}{}^2\mu_B{}^2}\chi_{Cu}} \qquad (2)$$

where z is the number of neighbors and J' is the magnitude of the interaction between interchain or interlayer Cu^{II} ions. The obtained parameter sets are summarized in Table 7, and the best fit with these parameters is represented as the solid line in Figure 12. The zJ' value of **10** is larger than that of **6**. As we can see in their structures (Figures 3 and 7), the nearest Cu···Cu distance is 5.12 Å for **10**, whereas that is 5.34 Å for **6**, the former being clearly shorter than the latter. Consequently, this structural difference affords the variation of magnitude of zJ' between **6** and **10**.

Conclusion

By using a metalloligand with multicoordination ability, $[Cu(2,4\text{-pydca})_2]^{2-}$ (L^{Cu}), as the building block, selective bond formation for first-period divalent transition metal ions has been accomplished: as $\{[ZnL^{Cu}(H_2O)_3(DMF)]\cdot DMF\}_n$ (**2**), $[ZnL^{Cu}(H_2O)_2(MeOH)_2]_n$ (**3**), $\{[ML^{Cu}(H_2O)_4]\cdot 2H_2O\}_n$ (M = Co (**4**), Cu (**5**), Zn (**6**)), and $\{[Cu(2,2'\text{-bpy})L^{Cu}]\cdot 3H_2O\}_n$ (**9**), the 4-carboxylate groups selectively bind with the present metal ions, and as $[ML^{Cu}(H_2O)_4]_n$ (M = Mn (**7**), Fe (**8**)), the 2-carboxylate groups selectively bind with the present metal ions. This may be related to the strength of Lewis-basicity and electrostatic effect of L^{Cu} and the Irving−Williams order on the present metal ions. Such a bonding selectivity of these compounds dramatically affects their magnetic properties: **4**, **5**, and **9** with the 4-carboxypyridinate bridge between magnetic centers showed weak antiferromagnetic interaction, and **7** and **8** with the carboxylate bridges on the contrary exhibited ferromagnetic behavior. It is worth noting that a control of properties characteristic of frameworks, for instance, magnetic properties, is attained by the use of L^{Cu} that potentially has the ability to identify first-period divalent transition metal ions. We anticipate this synthetic approach to be viable for the construction of desired coordination polymers, namely, crystal engineering of metalloligands.

Experimental Section

Materials. All chemicals and solvents used during the syntheses were reagent grade. $\{[Cu(2,2'\text{-bpy})_2]\cdot 2Cl\cdot 6H_2O\}_n$ was prepared according to the literature.[20] Compounds **2** and **3** were previously synthesized.[9]

Caution! Perchlorate salts are dangerous (especially if they are dry) and should be handled with care.

$[Cu(2,4\text{-pydcaH})_2(H_2O)_2]$ (1·2H). A methanol solution (300 mL) of 2,4-pydcaH_2 (3.34 g, 20.0 mmol) was added to an aqueous solution (50 mL) of $CuSO_4\cdot 5H_2O$ (2.50 g, 10.0 mmol). The obtained blue powder was collected by filtration, washed with methanol, and dried under vacuum for 1 h. Yield: 3.80 g (8.80 mmol, 88%). Anal. Calcd for $C_{14}H_{12}CuN_2O_{10}$: C, 39.12; H, 2.35; N, 6.52. Found: C, 38.30; H, 2.78; N, 6.35. IR (KBr pellet): 3406 m, 1728 s, 1635 s, 1610 s, 1562 m, 1477 w, 1433 w, 1367 s, 1282 s, 1257 s, 1182 m, 1093 w, 1035 w, 997 w, 902 w, 873 w, 810 w, 765 w, 721 m, 686 m, 574 w, 530 w, 472 w cm^{-1}.

The single crystals suitable for X-ray analysis were prepared by the careful diffusion of a methanol solution of 2,4-pydcaH_2 into an aqueous solution of $CuSO_4\cdot 5H_2O$.

$(Et_3NH)_2[Cu(2,4\text{-pydca})_2(H_2O)]$ (1·2Et$_3$NH). An excess triethylamine solution was added to a DMF suspension (30 mL) of **1**·2H (1.00 g, 2.31 mmol). To the resulting thick, blue solution was added an excess of acetone solution. The obtained blue powder was collected by filtration, washed with acetone, and dried under vacuum for 1 h. Yield: 1.37 g (2.22 mmol, 96%) Anal. Calcd for $C_{26}H_{40}CuN_4O_9$: C, 50.68; H, 9.09; N, 6.54. Found: C, 50.46; H, 9.07; N, 6.31. IR (KBr pellet): 3379 mb, 2976 m, 2939 m, 2739 m, 2677 m, 2492 m, 1658 s, 1628 s, 1614 s, 1554 m, 1469 m, 1435 w, 1369 m, 1342 s, 1263 m, 1161 w, 1035 m, 825 w, 781 m, 734 m, 694 m cm^{-1}.

The single crystals suitable for X-ray analysis were prepared by the careful diffusion of an acetone solution into a DMF solution of **1**·2H and excess Et_3N.

$\{[CoL^{Cu}(H_2O)_4]\cdot 2H_2O\}_n$ (4). An acetonitrile solution (20 mL) of $Co(BF_4)_2\cdot 6H_2O$ (218 mg, 0.640 mmol) was slowly diffused into an aqueous solution (20 mL) of **1**·2Et$_3$NH (200 mg, 0.325 mmol). The bluish-purple crystals were obtained after a few weeks, washed with methanol, and dried in air. Yield: 58 mg (0.103 mmol, 32%). Anal. Calcd for $C_{14}H_{18}CoCuN_2O_{14}$: C, 29.99; H, 3.24; N, 5.00. Found: C, 29.92; H, 3.18; N, 5.06. IR (KBr pellet): 3368 mb, 1645 s, 1616 s, 1558 m, 1477 w, 1392 m, 1336 s, 1257 m, 1095 w, 1035 w, 843 w, 773 m, 740 m, 690 m, 669 w, 574 w, 468 w cm^{-1}.

$\{[CuL^{Cu}(H_2O)_4]\cdot 2H_2O\}_n$ (5). A H_2O/methanol mixed solution (4 mL + 16 mL) of $Cu(AcO)_2\cdot H_2O$ (200 mg, 1.00 mmol) was slowly diffused into an aqueous solution (20 mL) of **1**·2Et$_3$NH (616 mg, 1.00 mmol) at room temperature. After a week, the obtained blue crystals were filtered, washed with methanol, and dried in air. Yield: 98 mg (0.067 mmol, 17%). Anal. Calcd for $C_{14}H_{18}Cu_2N_2O_{14}$: C, 29.74; H, 3.21; N, 4.95. Found: C, 30.17; H, 2.80; N, 5.02. IR (KBr pellet): 3373 mb, 1643 s, 1614 s, 1556 m, 1477 w, 1392 m, 1336 s, 1257 m, 1095 w, 1035 w, 841 w, 773 m, 740 m, 690 m, 584 w, 466 w cm^{-1}.

$\{[ZnL^{Cu}(H_2O)_4]\cdot 2H_2O\}_n$ (6). A methanol solution (10 mL) of $Zn(NO_3)_2\cdot 6H_2O$ (149 mg, 0.500 mmol) was slowly diffused into an aqueous solution (10 mL) of **1**·2Et$_3$NH (308 mg, 0.500 mmol). After a few weeks, the obtained blue crystals were collected, washed with methanol, and dried in air. Yield: 240 mg (0.423 mmol, 85%). Anal. Calcd for $C_{14}H_{18}CuN_2O_{14}Zn$: C, 29.64; H, 3.20; N, 4.94.

(20) Hathaway, B. J.; Procter, I. M.; Slade, R. C.; Tomlinson, A. A. G. *J. Chem. Soc. A* **1969**, 2219−2224.

Found: C, 29.63; H, 2.94; N, 4.94. IR (KBr pellet): 3350 mb, 1645 s, 1616 s, 1558 m, 1477 w, 1392 m, 1336 s, 1259 m, 1093 w, 1037 w, 881 w, 839 w, 775 m, 740 m, 690 m, 669 w, 617 w, 466 w cm^{-1}.

$[MnL^{Cu}(H_2O)_4]_n$ (7). A H_2O/methanol solution (4 mL + 16 mL) of $MnSO_4 \cdot 5H_2O$ (242 mg, 1.00 mmol) was carefully diffused to an aqueous solution (20 mL) of **1**·2Et_3NH (616 mg, 1 mmol). After a few weeks, the obtained purple crystals were filtered, washed with methanol, and dried in air. Yield: 104 mg (0.200 mmol, 20%). Anal. Calcd for $C_{14}H_{14}CuMnN_2O_{12}$: C, 32.29; H, 2.71; N, 5.38. Found: C, 31.86; H, 2.77; N, 5.30. IR (KBr pellet): 3383 mb, 3067 m, 1630 s, 1610 s, 1583 s, 1549 m, 1475 m, 1444 w, 1377 s, 1363 s, 1275 w, 1261 m, 1103 w, 1035 w, 825 w, 787 m, 733 m, 692 m, 569 w, 478 w cm^{-1}.

$[FeL^{Cu}(H_2O)_4]_n$ (8). A methanol solution (10 mL) of $Fe(ClO_4)_2 \cdot 6H_2O$ (182 mg, 0.500 mmol) was carefully diffused to an aqueous solution (10 mL) of **1**·2Et_3NH (308 mg, 0.500 mmol). After a few weeks, the light-brown crystals were obtained with another unidentified byproduct. After filtration, the mixture was separated by hand, and crystals were washed with methanol and dried in air. Yield: 62 mg (0.119 mmol, 24%). Anal. Calcd for $C_{14}H_{14}CuFeN_2O_{12}$: C, 32.23; H, 2.71; N, 5.37. Found: C, 31.93; H, 2.70; N, 5.35. IR (KBr pellet): 3368 wb, 3211 wb, 3069 w, 1630 s, 1610 s, 1583 s, 1549 m, 1475 m, 1444 w, 1378 s, 1363 s, 1275 w, 1261 m, 887 w, 833 w, 787 m, 733 m, 713 m, 688 m, 572 w, 480 w cm^{-1}.

$\{[Cu(2,2'\text{-bpy})L^{Cu}] \cdot 3H_2O\}_n$ (9). A methanol solution (20 mL) of $\{[Cu(2,2'\text{-bpy})_2] \cdot 2Cl \cdot 6H_2O\}$ (180 mg, 0.324 mmol) was added to a methanol solution (20 mL) of **1**·2Et_3NH (200 mg, 0.324 mmol). When the resulting blue solution was allowed to stand for 1 day, the bluish-purple microcrystals were obtained, filtered, washed with methanol, and dried in air. Yield: 119 mg (0.178 mmol, 55%). Anal. Calcd for $C_{24}H_{20}Cu_2N_4O_{11}$: C, 43.18; H, 3.02; N, 8.39. Found: C, 42.39; H, 2.93; N, 8.24. IR (KBr pellet): 3472 mb, 1643 s, 1608 s, 1556 m, 1471 m, 1448 w, 1383 m, 1342 s, 1273 w, 1261 m, 1157 w, 781 m, 772 m, 742 m, 731 w, 700 m, 667 w, 648 w, 445 w cm^{-1}.

The single crystals suitable for X-ray analysis were prepared by the careful diffusion of a methanol solution of $\{[Cu(2,2'\text{-bpy})_2] \cdot 2Cl \cdot 6H_2O\}$ into a methanol/ethylene glycol mixed solution of **1**·2Et_3NH.

$[Ag_2L^{Cu}]_n$ (10). A methanol solution (10 mL) of **1**·2Et_3NH (154 mg, 0.250 mmol) was carefully diffused to an aqueous solution (10 mL) of $AgBF_4$ (98 mg, 0.500 mmol). After a few days, the obtained purple crystals were filtered, washed with methanol, and dried under vacuum for 1 h. Yield: 133 mg (0.218 mmol, 87%). Anal. Calcd for $C_{14}H_6Ag_2CuN_2O_8$: C, 27.59; H, 0.99; N, 4.60. Found: C, 27.21; H, 1.16; N, 4.53. IR (KBr pellet): 3445 mb, 1633 s, 1608 s, 1585 s, 1547 s, 1477 m, 1373 s, 1342 s, 1263 m, 1190 w, 1086 m, 1039 w, 951 w, 875 w, 829 w, 775 m, 736 m, 688 m, 437 w cm^{-1}.

Physical Measurements. Elemental analyses were taken on Yanaco C,H,N Corder MT-5. IR spectra were recorded on a Hitachi I-5040FT-IR spectrometer with samples prepared as KBr pellets. General magnetic susceptibility data for samples were measured over the temperature range 1.82−300 K using an MPMS-XL SQUID susceptometer (Quantum Design, Inc.), where the applied magnetic fields were 1 kOe. Corrections were made for diamagnetism using Pascal's constants[3a] and for vinyl capsule wrapping samples.

X-ray Structure Determination. Single crystals of all compounds were mounted on a glass fiber and coated with epoxy resin. For **1**·2Et_3NH, **4**, and **7**−**10**, all measurements were made on a Rigaku RAXIS-RAPID imaging plate diffractometer with graphite monochromated Mo Kα radiation. For **1**·2H, all measurements were made on a Rigaku AFC7R diffractometer with graphite monochromated Mo Kα radiation and a rotating anode generator. Cell constants and an orientation matrix for data collection were obtained from a least-squares refinement using the setting angles of 25 carefully centered reflections in the range $29.69° < 2\theta < 29.96°$. For **5** and **6**, X-ray data collections were carried out by a Rigaku Mercury charge coupled device (CCD) system with graphite monochromated Mo Kα radiation. For **1**·2H, the structure was solved by a direct method using the SHELXS86 program[21] and expanded using Fourier techniques.[22] For **1**·2Et_3NH, **4**, **7**, and **9**, the structures were solved by a direct method using the SIR92 program[23] and expanded using Fourier techniques.[22] For **5** and **6**, the structures were solved by using the final atomic coordinate of the isomorphous **4** as an initial coordinate and expanded using Fourier techniques.[22] For **8**, the structure was solved by using the final atomic coordinate of the isomorphous **7** as an initial coordinate and expanded using Fourier techniques.[22] For **10**, the structure was solved by heavy-atom Patterson methods using the PATTY program[22] and expanded using Fourier techniques.[22] In all compounds, the non-hydrogen atoms were refined anisotropically. All hydrogen atoms, which were placed in idealized positions, were included but not refined. By way of exception, the H(4) and H(8) (4-carboxylic acid protons for **1**·2H), and the H(19) (triethylammonium proton for **1**·2Et_3NH), were observed from a Fourier map and fixed. The refinements were carried out using full-matrix least-squares techniques. All calculations were performed using the teXsan[24] crystallographic software package from the Molecular Structure Corporation. Crystal data and details of the structure determinations are summarized in Table 8.

Acknowledgment. This work was supported by Grant-in-Aid for Creative Scientific Research (13GS0024), the Ministry of Education, Culture, Sports, Science, and Technology of Japan. One of the authors (S.-i.N.) expresses gratitude to RIKEN for supporting him under a Special Postdoctoral Researchers Program.

Supporting Information Available: X-ray crystallographic files of **1**·2Et_3NH, **1**·2H, and **4**−**10**, in CIF format. This material is available free of charge via the Internet at http://pubs.acs.org.

IC049550E

(21) Sheldrick, G. M. In *Crystallographic Computing 3*; Sheldrick, G. M., Kruger, C., Goddard, R., Eds.; Oxford University Press: Oxford, 1985; pp 175−189.
(22) Beurskens, P. T.; Admiraal, G.; Beurskens, G.; Bosman, W. P.; Garcia-Granda, S.; Gould, R. O.; Smits, J. M. M.; Smykalla, C. *The DIRDIF Program System*; Technical Report of the Crystallography Laboratory; University of Nijmegen: Nijmegen, The Netherlands, 1992.
(23) Altomare, A.; Burla, M. C.; Camalli, M.; Cascarano, M.; Giacovazzo, C.; Guagliardi, A.; Polidori, G. *J. Appl. Crystallogr.* **1994**, *27*, 435.
(24) *teXsan: Crystal Structure Analysis Package*; Molecular Structure Corporation: The Woodlands, TX, 1985 and 1999.